HYPER-SET: DESIGNING TRANSFORMERS VIA HYPERSPHERICAL ENERGY MINIMIZATION

Anonymous authors
Paper under double-blind review

ABSTRACT

Transformer-based models have achieved remarkable success, but their core components, Transformer layers, are largely heuristics-driven and engineered from the bottom up, calling for a prototypical model with high interpretability and practical competence. To this end, we conceptualize a principled, top-down approach grounded in energy-based interpretation. Specifically, we formalize token dynamics as a joint maximum likelihood estimation on the hypersphere, featuring two properties: semantic alignment in the high-dimensional space and distributional uniformity in the low-dimensional space. By quantifying them with extended Hopfield energy functions, we instantiate this idea as a constrained energy minimization problem, which enables designs of symmetric attention and feedforward modules with RMS normalization. We further present *Hyper-Spherical Energy Transformer* (HYPER-SET), a recurrent-depth alternative to vanilla Transformers naturally emerging from iterative energy optimization on the hypersphere. With shared parameters across layers, HYPER-SET can scale to arbitrary depth with fewer parameters. Theoretically grounded and compact, it achieves competitive or superior performance across diverse tasks, including Sudoku solving, image classification, and masked image modeling. We also design novel variations under the proposed general principle, such as linear attention and gated feedforward layer, and showcase its scalability with depth-wise LoRA. Our results highlight HYPER-SET as a step toward interpretable and principled Transformer design.

1 INTRODUCTION

Transformer-based models (Vaswani et al., 2017) have become foundational across diverse domains, including computer vision (Dosovitskiy et al., 2021; Bao et al., 2022; He et al., 2022; Peebles & Xie, 2023), natural language (Devlin et al., 2019; Lan et al., 2020; Brown et al., 2020), robotics (Brohan et al., 2022; Chen et al., 2021), and scientific discovery (Jumper et al., 2021; Kamienny et al., 2022). In recent years, there has been evidence that scaling up model size, dataset size, or computational budget during pre-training can yield unprecedented performance gains (Kaplan et al., 2020), driving the proliferation of Transformer-based foundation models (OpenAI et al., 2024; Dubey et al., 2024; Anil et al., 2023; Oquab et al., 2024).

Despite these achievements, the architecture of Transformers—especially the configurations and role of individual layers—remains largely heuristic. For instance, empirical studies have observed high redundancy in the deeper layers (Gromov et al., 2024; Men et al., 2024), uniformity of representations in the middle layers (Sun et al., 2024), and robustness to permuting certain intermediate layers (Lad et al., 2024) in LLMs. These findings suggest convergent functionality that one layer represents, yet our understanding of its role in processing information and representation learning remains limited. While interpretability efforts to unveil the function underlying the network layers exist, especially Transformer blocks-ranging from mechanistic interpretability (Elhage et al., 2021; Nanda et al., 2023; Wang et al., 2023; Huben et al., 2024) to causal mediation analysis (Vig et al., 2020; Meng et al., 2022) and visualization (Bricken et al., 2023; Olsson et al., 2022)-most focus on *post hoc* interpretation and phenomenological approaches. This motivates a pivotal question:

Can we find or design a function prior that induces a model that is interpretable by construction?

One approach to achieving intrinsic interpretability is to embed an explicit optimization process into neural networks, known as model-based deep learning (Shlezinger et al., 2023). Prior works have designed networks that solve domain-specific problems such as constraint satisfaction (Wang et al., 2019), optimal control (Amos & Kolter, 2017; Amos et al., 2018), or physical simulation (Greydanus et al., 2019; Karniadakis et al., 2021). However, these models often rely on fixed task priors and lack generality.

Another more general avenue is energy-based learning (EBL) (Dawid & LeCun, 2024), which frames prediction as minimizing a scalar energy function $E_\theta(x, y)$ over outputs y conditioned on inputs x. Within this framework, Energy Transformer (Hoover et al., 2024) interprets Transformer layers as iterative optimization over the canonical continuous Hopfield energy (Ramsauer et al., 2021; Krotov & Hopfield, 2021) yet focuses on mechanistic analogies to associative memory without grounding its formulation in specific representational challenges. In contrast, our goal is to find a design principle from top down that can not only reinterpret existing components but is also generalizable to novel architecture design *constructively*.

In this work, we therefore take a fundamentally different approach by introducing a principle grounded in maximum likelihood estimation (MLE) for tokens on the hypersphere. Under mild assumptions, we interpret it under two complementary objectives for representation dynamics: semantic alignment (mode seeking) in high-dimensional space and distributional uniformity (mass covering) in a low-dimensional subspace. To translate these objectives into optimizable quantities over tokens, we define two complementary Hopfield-style energy functions that quantify these objectives and can be minimized through iterative optimization. This leads to the *Hyper-Spherical Energy Transformer* (HYPER-SET)—a recurrent-depth model in which core components such as symmetric attention, feedforward layers, $\mathrm{RMSNorm}$, and skip connection emerge naturally from the optimization dynamics. With only one set of shared parameters across iterations, HYPER-SET is compact, interpretable by design, and empirically competitive across diverse tasks, including reasoning, classification, and masked image modeling. Beyond a single instantiation, this principle can induce novel architectural designs by generalizing the energy functions, enabling variants such as linear attention and gated feedforward layer. To enhance scalability, we introduce depth-wise low-rank adaptation (LoRA), allowing flexible iteration-specific modulation with minimal parameter overhead. Our key contributions are summarized as follows:

1. **Theoretical Formulation**: We conceptualize a general principle for information processing in layer dynamics based on maximum likelihood estimation on the hypersphere with two properties: uniformity and alignment, quantified via complementary Hopfield-style energy functions.
2. **Energy-Driven Architecture**: We derive a compact Transformer-based model through pure energy minimization, where core components—including symmetric attention, feedforward, $\mathrm{RMSNorm}$ (Zhang & Sennrich, 2019), and skip connection—emerge naturally.
3. **Competitive Performance**: We show competitive performance to vanilla Transformer across reasoning, classification, and masked modeling while demonstrating generality to design novel components (*e.g.*, linear attention, gated feedforward) and scalability with flexible computation.

2 Related Work

2.1 Energy-based Learning

Energy-based learning (EBL) (LeCun et al., 2006; Dawid & LeCun, 2024) provides a unifying framework for modeling prediction as minimizing an energy function. Early forms include Hopfield networks (Hopfield, 1982) and Boltzmann machines (Ackley et al., 1985). Modern developments in EBL span both generative modeling—via energy functions (Du & Mordatch, 2019) or their gradients (as in score-based models (Sohl-Dickstein et al., 2015; Song & Ermon, 2019))—and representation learning. Another line of work views network layers as the result of iterative energy minimization. Some approaches define energy implicitly through neural networks (Bai et al., 2019; Du et al., 2022; 2024), while recent work Energy Transformer (Hoover et al., 2024) draws analogies between attention layers and explicit energy descent but mainly focuses on reinterpretation rather than principled derivation. Our work differs in that we design the Transformer block by quantifying a general principle that can induce variants through alternative energy.

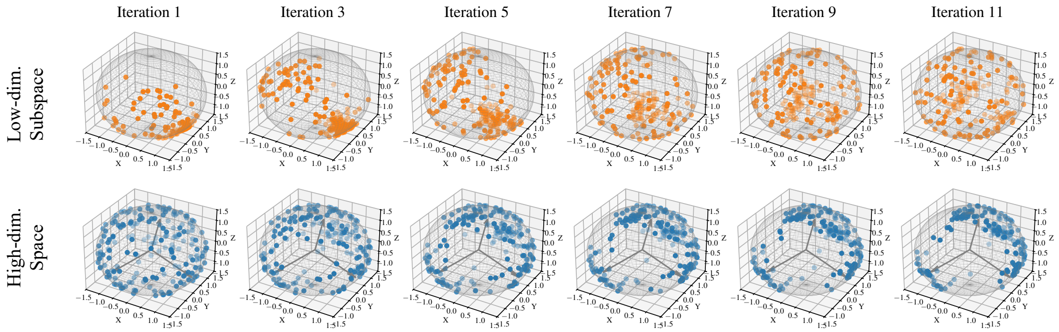

Figure 1: Evolution of tokens in the forward pass. *Top*: Tokens projected onto subspaces are progressively separated on the **low-dimensional** hypersphere. *Bottom*: Tokens gradually align with anchor vectors in the **high-dimensional** hypersphere. Visualization is carried out in three-dimensional space for illustrative purposes.

Other works also explore energy formulations on the hypersphere (Liu et al., 2018; Loshchilov et al., 2024), but mostly in the weight space. By contrast, we define our energies directly on the representation space. Additionally, recent theoretical studies on memory capacity in modern Hopfield networks (Hu et al., 2024a; Wu et al., 2024a; Hu et al., 2024b) emphasize spreading patterns on the sphere but focus primarily on memory retrieval and cross-attention.

2.2 Model Design from First Principles

While neural network architectures are often shaped by engineering practices, recent work has explored designing or interpreting them through principled lenses like signal processing, information theory, and neurobiology. For example, deep unrolling of the sparse coding algorithms has led to the development of fully connected networks (Gregor & LeCun, 2010), convolution networks (Papyan et al., 2017; 2018), and even graph neural networks through iterative algorithms (Yang et al., 2021). Similarly, the sparse rate reduction principle has been used to derive the Transformer architecture (Yu et al., 2023). Other approaches draw inspiration from approximation theory (Liu et al., 2024) and brain computation (Kozachkov et al., 2023), further bridging the gap between theoretical insights and practical network design.

2.3 Depth Recurrence in Transformers

Recurrence has been scientifically considered as a core computational mechanism in the biological visual system enabling flexible computational depth, integration of priors, and efficient allocation of compute under resource constraints (van Bergen & Kriegeskorte, 2020). Depth-wise recurrence in Transformer architectures, under the name of universal (Devlin et al., 2019), recursive/recurrent (Bae et al., 2025; Geiping et al., 2025) or looped Transformers (Giannou et al., 2023), where cross-layer weights are shared, has emerged as a critical avenue for reducing parameters and enabling iterative reasoning. Its repeated reuse of the same layer has been demonstrated capable of emulating iterative algorithms Schwarzschild et al. (2021); Saunshi et al. (2025). Crucially, it has been demonstrated with particular strength mostly on systematic generalization (Csordás et al., 2021) and structured reasoning tasks (Schwarzschild et al., 2021; Bansal et al., 2022), while its applications on general-domain tasks that need hierarchical processing (e.g, image perception) are under-explored.

3 Conceptualization and Instantiation

To answer the introductory question, we conjecture that effective representations should exhibit two complementary properties: **semantic alignment** in a high-dimensional space and **distributional uniformity** in a low-dimensional subspace. This dual perspective reflects the balance of *mode seeking* and *mass covering*—terms we use to characterize the interplay between information preservation and entropy collapse prevention in representation learning. Figure 1 shows an illustrative example.

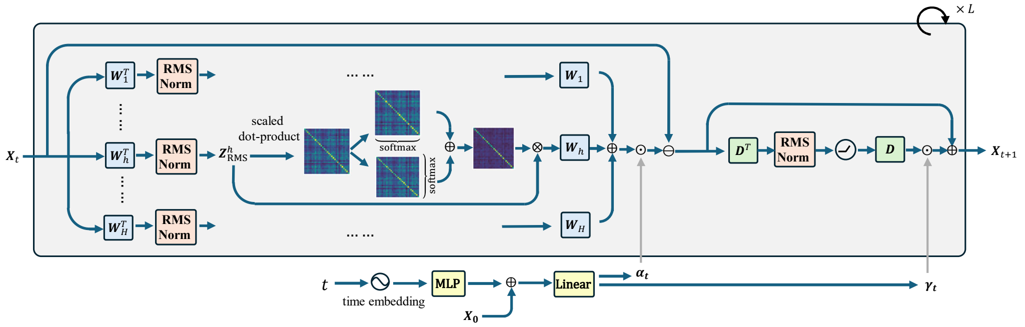

Figure 2: Overview of hyperspherical energy Transformer layer. It recovers sequential stacking of symmetric self-attention, feedforward, skip connection, and $\mathrm{RMSNorm}$ from sheer minimization of extended Hopfield energy. Adaptive step sizes are learned given the current t and initial input $\boldsymbol{X}_0$.

We formalize this conceptualization under maximum likelihood estimation. Specifically, we instantiate the forward dynamics as an optimization over a token-level vector $\boldsymbol{x}$ balancing two terms:

$$\min_{\boldsymbol{x}} \quad \underbrace{\sum_{h=1}^{H} \mathrm{D}_{\mathrm{KL}}(p(\boldsymbol{z}) \| p_\phi(\boldsymbol{z}^h | \boldsymbol{x}))}_{\text{uniformity}} \underbrace{- \log p_\theta(\boldsymbol{x})}_{\text{alignment}}, \tag{1}$$

where $\boldsymbol{z}^h$ represents low-dimensional projections of the high-dimensional representation $\boldsymbol{x}$.

The first term encourages the projections $\boldsymbol{z}^h$ to approximate a prior uniform distribution $p(\boldsymbol{z})$ on a hypersphere, thus maximizing entropy and mitigating representational collapse. The second term promotes alignment between $\boldsymbol{x}$ and mean directions, which can be modeled using von Mises–Fisher distributions. A detailed justification and interpretation of this objective is provided in Appendix A.

This objective resonates with but differs from the contrastive learning objective that unifies alignment and uniformity in a shared latent space (Wang & Isola, 2020). Our work instead takes on an energy view to quantify these two key ingredients into optimizable functions of $\boldsymbol{x}$ that can induce Transformer architectures.

4 Hyperspherical Energy Transformer from Iterative Energy Minimization

In this section, we translate the proposed instantiation into two modified Hopfield energy functions defined on hyperspheres (see Appendix B for preliminaries and definition of Hopfield energy E_{MCH} in Eq. 16). Through iterative energy minimization, the architectural components of Transformer layers naturally arise under this framework. The overview is presented in Figure 2.

4.1 Hyperspherical Energy

Let $\boldsymbol{X} = [\boldsymbol{x}_1, \ldots, \boldsymbol{x}_N]$ denote a set of N contextual token vectors, each $\boldsymbol{x}_i \in \mathbb{R}^d$. These tokens are projected into H distinct subspaces via basis matrices $\boldsymbol{W} = [\boldsymbol{W}_1, \ldots, \boldsymbol{W}_H] \in \mathbb{R}^{d \times Hp}$, where each $\boldsymbol{W}_h \in \mathbb{R}^{d \times p}$ spans a p-dimensional subspace. Additionally, we define a second set of bases $\boldsymbol{D} = [\boldsymbol{d}_1, \ldots, \boldsymbol{d}_M] \in \mathbb{R}^{d \times M}$ to encode semantic directions in the original space. Unless otherwise specified, we assume these basis vectors are incoherent and span the full space, *i.e.*, $Hp = M = d$.

4.1.1 Overcoming Token Synchronization via Repulsive Dynamics

Motivated by a recent argument that the contextual tokens lie on a low-dimensional manifold of their high-dimensional ambient space (Yu et al., 2023), we study the projection of tokens with bases $\boldsymbol{W}$; for a subspace spanned by $\boldsymbol{W}_h$, the latent representation of a token $\boldsymbol{x}_i$ can be written as

$$\boldsymbol{z}_i^h = \boldsymbol{W}_h^T \boldsymbol{x}_i. \tag{2}$$

Canonical Hopfield energy E_{MCH} tends to align vectors with stored patterns. This interaction often occurs between dynamic tokens and static patterns. However, in Transformers' self-attention, this interplay happens among all dynamic tokens simultaneously. Enforcing strict alignment among them risks collapsing representations into degenerate clusters, reducing expressiveness. This phenomenon has been observed empirically as oversmoothing (Chen et al., 2022; Wu et al., 2024b) or rank collapse (Dong et al., 2021), and theoretically characterized in (Geshkovski et al., 2023). It also relates to the synchronization effect in coupled systems (Acebrón et al., 2005; Miyato et al., 2024).

Therefore, to overcome this issue, we extend the Hopfield energy E_{MCH} to model the repulsive force among tokens and quantify their distributional uniformity in each subspace, which serves as a surrogate of the uniformity measure in Eq. 1. For subspace h, this energy is given by

$$E^h_{\text{ATTN}} = \beta^{-1} \sum_{i=1}^{N} \log\Big(\sum_{j=1}^{N} \exp\big(\beta(\boldsymbol{z}_i^h)^T(\boldsymbol{z}_j^h)\big)\, , \tag{3}$$

where β is usually the inverse of temperature. Here we use the subscript $_{\text{ATTN}}$ as this energy will be shown to be related to the design of the attention layer, resembling that in (Yu et al., 2023). Aggregating over all subspaces, the total energy that models interacting tokens would be

$$E_{\text{ATTN}} = \sum_{h=1}^{H} E^h_{\text{ATTN}}, \quad \text{subject to } \|\boldsymbol{W}_h^T \boldsymbol{x}_i\|_2 = \sqrt{p}. \tag{4}$$

The constraint ensures that the dynamics take place on a low-dimensional hypersphere of radius $\sqrt{p}$. Minimizing E_{ATTN} thus encourages token spread evenly on multiple hyperspheres, mitigating collapse and promoting distributional uniformity. [1]

4.1.2 Semantic Alignment via Attraction to High-Dimensional Bases

While the subspace projections separate to occupy more volume thus regularizing distribution, we seek to enrich the high-dimensional representations per se. From an information-theoretic perspective (Tishby et al., 2000; Tishby & Zaslavsky, 2015), effective representations require compressing uninformative redundancy while preserving salient information. Hence, in the original high-dimensional space, we encourage token alignment with a set of directions that contain knowledge from data to reduce entropy for minimal coding bits.

Motivated by empirical findings that feedforward layers in Transformers store much of their knowledge (Geva et al., 2021; Dar et al., 2023), we interpret the basis vectors $\boldsymbol{D}$ as the semantic directions. One surrogate function to implement this attractive energy for alignment in Eq. 1 is defined as

$$E_{\text{FF}} = -\frac{1}{2} \sum_{i=1}^{N} \sum_{m=1}^{M} \left(\text{ReLU}\left(\boldsymbol{d}_m^T \boldsymbol{x}_i\right)\right)^2, \quad \text{subject to } \|\boldsymbol{D}^T \boldsymbol{x}_i\|_2 = \sqrt{M}. \tag{5}$$

Here we use the subscript $_{\text{FF}}$ as this energy relates to the design of the feedforward layer. This energy favors alignment between tokens and those basis directions forming acute angles (as filtered by ReLU), while maintaining the hyperspherical constraint in the original space. Geometrically, each token is drawn toward a union of attractive half-spaces defined by $\boldsymbol{D}$. This could imply that each token may bind patterns combinatorially beyond the number of basis vectors defined by $\boldsymbol{D}$.

4.1.3 Dual Energy on the Hypersphere

By combining these two hyperspherical energy functions, we introduce a unified objective function that characterizes the functionality the Transformer layer represents:

$$\min_{\boldsymbol{x}_1,\ldots,\boldsymbol{x}_N \in \boldsymbol{X}} \quad E(\boldsymbol{X}; \boldsymbol{W}, \boldsymbol{D}) = E_{\text{ATTN}} + E_{\text{FF}} \tag{6}$$
$$\text{subject to} \quad \|\boldsymbol{W}_h^T \boldsymbol{x}_i\|_2 = \sqrt{p}, \quad \|\boldsymbol{D}^T \boldsymbol{x}_i\|_2 = \sqrt{M}, \quad i = 1, \ldots, N.$$

Iteratively minimizing this energy under spherical constraints induces the core architecture of Transformer layers: self-attention module arises from repulsive energy over subspaces and feedforward module arises from attractive energy in the ambient space. To solve optimization Eq. 6, we adopt an alternating minimization method by splitting it into sub-problems, following (Yu et al., 2023).

[1] Its asymptotic convergence to uniformity on the sphere has been proven in (Liu et al., 2018).

4.2 Symmetric Structure Induced From Energy Minimization

4.2.1 Attention Module from Uniform Energy

To show how we have an attention module derived from minimizing hyperspherical energy E_{ATTN} in Eq. 4, we first establish the differential equation that models the evolution of tokens' interactions:

$$\begin{aligned}\dot{\boldsymbol{X}} &= -\nabla_{\boldsymbol{X}} E_{\text{ATTN}} \\ &= -\sum_{h=1}^{H} \boldsymbol{W}_h \boldsymbol{W}_h^T \boldsymbol{X} \left(\underbrace{\text{softmax}}_{\text{column-wise}} \left(\beta (\boldsymbol{W}_h^T \boldsymbol{X})^T (\boldsymbol{W}_h^T \boldsymbol{X})\right) + \underbrace{\text{softmax}}_{\text{row-wise}} \left(\beta (\boldsymbol{W}_h^T \boldsymbol{X})^T (\boldsymbol{W}_h^T \boldsymbol{X})\right) \right)\end{aligned} \tag{7}$$

where $\beta = 1/\sqrt{p}$ as in vanilla Transformers. Derivations could be found in Appendix C.1.

The constraint on the low-dimensional hypersphere of radius $\sqrt{p}$ corresponds to $\text{RMSNorm}(\cdot)$, which bears resemblance to Query-Key Normalization (Henry et al., 2020), but here the normalization is applied after projection by the same query-key-value matrix. The projections in subspace h onto the hypersphere thus read as

$$\boldsymbol{Z}^h_{\text{RMS}} = \text{RMSNorm}(\boldsymbol{Z}^h) = \text{RMSNorm}(\boldsymbol{W}_h^T \boldsymbol{X}). \tag{8}$$

By discretizing the differential equation Eq. 7 with step size α_t and maintaining the constraint Eq. 8, we obtain an self-attention module; let $[\boldsymbol{QK}]_{\text{RMS,t}} = \beta(\boldsymbol{Z}^h_{\text{RMS},t})^T(\boldsymbol{Z}^h_{\text{RMS},t})$, then the update will be:

$$\boldsymbol{X}_{t+1} = \boldsymbol{X}_t - \alpha_t \sum_{h=1}^{H} \left(\boldsymbol{W}_h \boldsymbol{Z}^h_{\text{RMS},t} \underbrace{\text{softmax}}_{\text{column-wise}} \left([\boldsymbol{QK}]_{\text{RMS,t}}\right) + \boldsymbol{W}_h \boldsymbol{Z}^h_{\text{RMS},t} \underbrace{\text{softmax}}_{\text{row-wise}} \left([\boldsymbol{QK}]_{\text{RMS,t}}\right) \right). \tag{9}$$

This update yields a doubly symmetric multi-head attention operator, where both the query-key dot product and attention weights are symmetric under row and column operations. This structure connects with formulations of Wasserstein gradient flows using doubly stochastic attention (Sander et al., 2022), grounding our energy-based interpretation.

4.2.2 Feedforward Module from Alignment Energy

For the sub-problem of minimizing the alignment energy E_{FF} in Eq. 5, we have a similar construction of the corresponding differential equation, with details deferred to Appendix C.2:

$$\dot{\boldsymbol{X}} = -\nabla_{\boldsymbol{X}} E_{\text{FF}} = \boldsymbol{D}\, \text{ReLU}\left(\boldsymbol{D}^T \boldsymbol{X}\right). \tag{10}$$

By further imposing the high-dimensional hyperspherical constraint via RMSNorm with discretization step size γ_t, we can recover the feedforward layer that exhibits symmetry in the weight space:

$$\boldsymbol{X}_{t+1} = \boldsymbol{X}_t + \gamma_t \boldsymbol{D}\, \text{ReLU}\left(\text{RMSNorm}\left(\boldsymbol{D}^T \boldsymbol{X}_t\right)\right). \tag{11}$$

4.3 Learning Adaptive Step Size

To make the step sizes more flexible, we choose to learn their embedding with a neural network conditioned on the current iteration t and the initial token $\boldsymbol{x}(0)$ (usually the output of the tokenizer):

$$\alpha_t = \boldsymbol{\alpha}_\eta(t, \boldsymbol{x}(0)), \quad \gamma_t = \boldsymbol{\gamma}_\psi(t, \boldsymbol{x}(0)). \tag{12}$$

For each iteration, step size embeddings in Eq. 12 are applied channel-wise to each token, similar to techniques in (Touvron et al., 2021; Peebles & Xie, 2023) and detailed in Appendix D.1. We also adopt the zero-initialization of network parameters η and ψ from (Bachlechner et al., 2021) to facilitate convergence when using larger iterations.

In summary, by combining all the components and techniques, we present the *Hyper-Spherical Energy Transformer* with only one layer of learnable parameters. This one-layer model is amenable to rigorous analysis and, as demonstrated later, has competitive performance with vanilla Transformer.

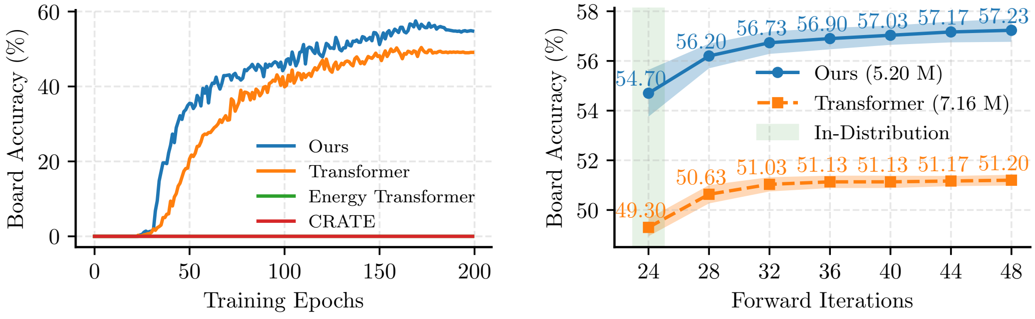

(a) Sudoku training dynamics

(b) Sudoku test-time extrapolation

Figure 3: *Left*: Training dynamics of different approaches. Ours has a superior training curve and converges faster, while Energy Transformer and CRATE both fail to make accurate predictions. *Right*: Test-time extrapolation w.r.t. forward iterations. Our model achieves better performance over five runs with fewer parameters, even when the iterations are beyond the training regime.

5 EXPERIMENT

In this section, we evaluate HYPER-SET against vanilla Transformer and other baselines on discriminative and generative tasks. For fairness, we remove biases and dropout, use the Pre-Norm style with RMSNorm, and set the MLP ratio to 4 in Transformer. We use one-layer trainable parameters but vary the forward iterations for all models, including Transformers, unless otherwise specified. [2]

5.1 SOLVING SUDOKU

Setups We use the challenging dataset from (Palm et al., 2018), featuring boards with only 17 to 34 known digits. We build on the code [3] from (Yang et al., 2023) and follow the setting of training on 9k samples and evaluating on 1k. See Appendix D.2 for details.

Extrapolation to Out-of-Distribution Iterations Under identical experimental conditions, our model exhibits faster and superior training dynamics over Transformer, while Energy Transformer (Hoover et al., 2024) and white-box Transformer CRATE (Yu et al., 2023) both fail on this task, as shown in Figure 3a. It also outperforms Transformer for in-distribution evaluation (54.70% vs. 49.30%), *i.e.*, using the same forward iterations for training and inference.

Recent efforts also explore test-time compute scaling to enhance reasoning (Schwarzschild et al., 2021; Bansal et al., 2022; Du et al., 2022; Banino et al., 2021), aiming to extrapolate the algorithms. Building on this idea, we increase test-time iterations up to 2× of training ones. As shown in Figure 3b, our model scales more effectively than Transformer, with larger accuracy gains. We attribute this extrapolation to learned adaptive step sizes that preserve energy minimization. In practice, we also find that trainable positional encoding is vital for the extrapolation.

Sudoku could be challenging for some architectures to achieve non-zero results, as the 9×9 grid requires the exact digits to meet the constraints, which may be hard to learn without proper inductive bias. Even some foundation models have zero accuracy (Wang et al., 2025). A reasonable explanation for HYPER-SET's success, where CRATE and Energy Transformer fail, is that we have better modeling and more realistic assumptions about the design objective, which is based on as fundamental as maximum likelihood, making the architecture better aligned with the optimization procedure. This allows HYPER-SET to enjoy both the principled design and the expressivity of Transformer.

5.2 IMAGE CLASSIFICATION

Setups & Results We also compare HYPER-SET on CIFAR-10/100, ImageNet-100, [4], and the full ImageNet-1K against ViTs, CRATE (Yu et al., 2023) its variant CRATE-T that aims for more

[2] For instance, 12 iterations mean applying the layer repeatedly 12 times.

[3] https://github.com/azreasoners/recurrent_transformer

[4] We use a subset of ImageNet-1K from https://github.com/HobbitLong/CMC/blob/master/imagenet100.txt

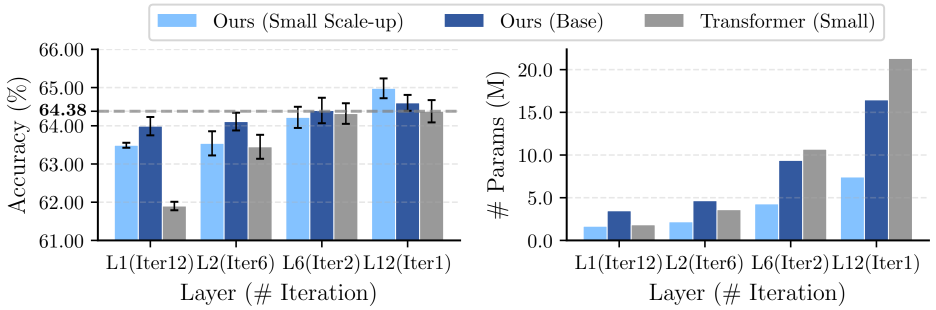

Figure 4: Top-1 accuracy (*Left*) and model parameters (*Right*) on CIFAR-100 with different layer-iteration trade-offs. Our model (Base) consistently surpasses Transformer, even its upper bound performance, with parameter efficiency. Error bars represent standard deviation over five runs.

faithful implementations (Hu et al., 2024c), and Energy Transformer (Hoover et al., 2024). Detailed setups are in Appendix D.3.

Table 1: Top-1 accuracy for image classification with single-layer recurrent-depth models. Parameters are measured on ImageNet-1K. All models are trained from scratch on listed datasets.

Models	Width d	# Params	Dataset			
			CIFAR-10	CIFAR-100	IN-100	IN-1K
Transformer	384	2.38 M	89.90	61.89	69.44	**66.94**
CRATE-T (Hu et al., 2024c)	896	3.04 M	87.54	60.23	68.16	57.89
CRATE (Yu et al., 2023)	768	3.00 M	84.81	58.22	68.52	57.00
Energy Transformer (Hoover et al., 2024)	512	2.39 M	76.39	50.60	36.68	34.24
Ours	512	2.39 M	**90.11**	63.41	**70.16**	62.76
Ours	640	3.40 M	89.96	**64.60**	69.31	66.21

Table 1 shows that, under properly parameter-aligned settings, our model surpasses others on CIFAR-10/100 and ImageNet-100 but lags behind Transformer on large-scale ImageNet-1K. Notably, our architecture achieves a higher width-parameter ratio compared to Transformer, meaning more parameter-efficient under the same width. [5] When scaling up the width d, our model can narrow the performance gap to Transformer. This implies that our principled model suits better under a resource-constrained setting as its inherent structural biases could limit its scaling on large datasets.

Layer-Iteration Trade-off So far, the classification is conducted using a one-layer model. A natural question is how well the model performs when stacking multiple layers with different parameters. To see this, we first train a Transformer with 12 layers—equivalent in effective depth to one layer with 12 iterations—as an upper bound. We then vary the number of distinct layers and their iterations while keeping total depth constant, effectively introducing flexibility to the basis vectors.

In Figure 4, our scaled-up `small` model has parameter efficiency across varied layer-iteration ratios, with this strength intensifying as more independent layers are trained. However, its architectural efficiency limits scalability beyond two layers. Scaling to the `Base` configurations enables our model to consistently outperform Transformer, exceeding the upper bound while retaining less parameters.

Non-Recurrent Scenarios To demonstrate the practicality in the non-recurrent settings, which are more common in large-scale applications, we further provide comparisons in a 12-layer non-recurrent setting in Table 2, where we report results on CIFAR-10/100 with fine-tuning or training from scratch and on large-scale ImageNet-1K. The ImageNet-1K pretraining setup follows Table 1, with fine-tuning batch size 256, epochs 50, learning rate 1e-4, and weight decay 1e-5. Our model performs comparably as standard Transformers while being more parameter-efficient, and this parameter reduction constantly grows when stacking more distinct layers, as shown in Figure 4, thanks to our parsimonious design. This suggests that HYPER-SET potentially preserves the benefit of scaling in Transformers when extended practically, while being more useful in resource-constrained settings where model size matters, further underscoring its promise in practical scenarios.

[5] We compare the parameter efficiency and computational cost in Appendix D.6.

Table 2: Top-1 accuracy for image classification with 12-layer non-recurrent-depth models. Parameters are measured on ImageNet-1K. * means first pretraining on ImageNet-1K and then fine-tuning on CIFAR-10/100.

Models	Width d	# Params	Dataset				
			CIFAR-10	CIFAR-100	CIFAR-10*	CIFAR-100*	IN-1K
Transformer	384	21.86 M	87.44	62.84	**96.95**	**83.10**	**67.90**
CRATE (Yu et al., 2023)	512	10.28 M	88.76	63.94	94.18	77.39	60.69
Ours	512	8.17 M	**88.82**	**64.98**	95.76	80.89	66.26
Ours	768	17.56 M	88.53	64.16	96.47	82.60	67.20

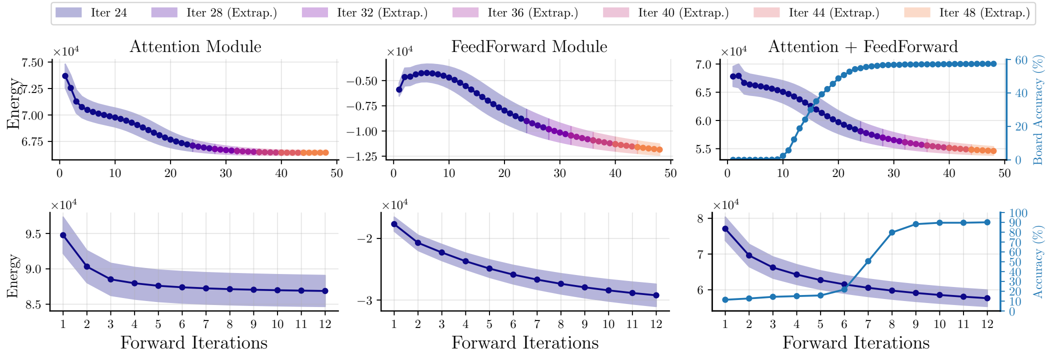

Figure 5: The attention and feedforward energy decrease on Sudoku (*Top*) and CIFAR-10 (*Down*) even without sign constraints on step sizes. This suggests the layer aligns well with the optimization objective. Normalization is first applied to meet constraints in Eq. 6 before computing the energy. In the right figure, the decrease in the overall energy corresponds to the increase in performance.

5.3 Masked Image Modeling

Setups & Results Masked image modeling has recently regained its traction for autoregressive generation (Li et al., 2023; 2024), framed as recovering images from 100% masking. Due to its high computational demand, we attempt to demonstrate the power of our one-layer model specifically for image reconstruction on ImageNet-100. We build on prior work (Chang et al., 2022) and use the open-source repository. [6] Concrete settings are in Appendix D.4, with additional results and visualization in Appendix E.

Table 3 unveils that, under the same number of iterations, our model significantly reduces parameters but lags behind Transformer on all metrics. If we further increase its iterations and the width of feedforward module M to $8d$, it can fill in the performance gap but at the cost of more computation.

Table 3: Comparisons of masked image modeling performance on ImageNet-100 (5k). Our model lags behind Transformer when given the same iterations, but matches its performance if scaling up the width of the feedforward module (larger M). Our model is also more parameter-efficient.

Models	Layer / Iteration / FF Ratio M	PSNR (↑)	SSIM (↑)	Multi-Scale SSIM (↑)	LPIPS (↓)	FID (↓)
Transformer	1 / 12 / $4d$ (8.85 M)	15.953	**0.417**	**0.599**	**0.327**	**43.428**
Ours	1 / 12 / d (3.94 M)	15.713	0.411	0.576	0.358	59.841
Ours	1 / 24 / $8d$ (8.07 M)	**15.955**	**0.417**	0.596	0.332	45.174

5.4 Energy Evolution, Effective Rank and Average Angle

Figure 5 shows energy trajectories of the attention (E_{ATTN}) and feedforward module (E_{FF}). Even without a positive threshold for step sizes α_t and γ_t, the energy on Sudoku still decreases within training iterations and extrapolates smoothly beyond them, indicating strong generalization of learned step sizes. On CIFAR-10, our designed energy exhibits a monotonic decline as well.

[6] https://github.com/valeoai/Maskgit-pytorch

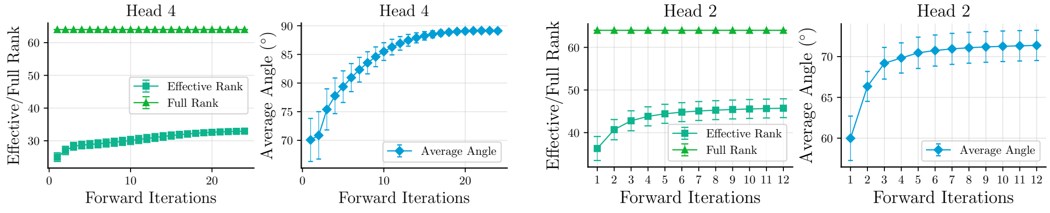

(a) Sudoku

(b) CIFAR-10

Figure 6: The effective rank and average angle of tokens projected to one subspace gradually increase, suggesting a larger volume spanned by these tokens. Results are from Sudoku test dataset (Palm et al., 2018) (*Left*) and CIFAR-10 validation set (*Right*).

To verify our subspace uniformity objective, we track two metrics—*effective rank* and *average angle*—defined in Appendix D.5. As shown in Figure 6, the subspace effective rank steadily increases while the full rank remains unchanged. Meanwhile, average angles between tokens approach orthogonality, aligning with our goal to prevent entropy collapse. Full results and comparisons with parameter-sharing Transformer are in Appendix F.

Table 4: Alternative designs on key components measured by top-1 accuracy for CIFAR-10 and CIFAR-100.

Components	Alternative Designs	Dataset	
		CIFAR-10	CIFAR-100
E_{ATTN}	Bi-Softmax Attention (Ours)	**90.11**	**63.41**
	Sigmoid Attention	85.93	59.72
	Linear Attention	84.88	56.97
E_{FF}	ReLU FF (Ours)	**90.11**	**63.41**
	Softmax FF	88.20	62.44
	Gated FF	84.99	59.29
Step Size	Learning Step Size (Ours)	**90.11**	**63.41**
	$\alpha_t = \gamma_t = 0.5$	25.81	57.92
	$\alpha_t = \gamma_t = 0.1$	81.45	58.29

Table 5: ImageNet-100 accuracy of HYPER-SET under different matrix rank within LoRA. Depth-wise LoRA introduces flexibility in the computation at each iteration.

Rank	# Params	Accuracy (%)
Ours	1.93 M	70.16
+ depth-wise LoRA (r=4)	2.03 M	70.36
+ depth-wise LoRA (r=8)	2.13 M	70.40
+ depth-wise LoRA (r=16)	2.33 M	70.56
+ depth-wise LoRA (r=32)	2.72 M	**72.20**

5.5 ALTERNATIVE DESIGNS AND SCALABILITY

A key strength of our formulation Eq. 1 lies in its generality—it supports a broad spectrum of model variants through alternative energy functions. For example, replacing the attention energy with a kernel-based function yields novel attention mechanisms, including linear attention. Similarly, gating in feedforward layers naturally arises by generalizing the feedforward energy. Table 4 shows the performance of these variants and results with different fixed step sizes, with details in Appendix G.1

To improve scalability with compact parameterizations, we introduce a lightweight extension inspired by (Bae et al., 2025), where learnable low-rank adapters are added at each forward iteration to modulate shared weights. This depth-wise adaptation, shown in Table 5, enhances performance without significantly increasing parameter count. Setups and additional scaling results on image and text modalities are included in Appendix G.2.

6 CONCLUSION

We present HYPER-SET, a Transformer architecture designed via iterative optimization of hyperspherical energy functions, bridging energy-based learning and practical model design. By formulating dual energy on the hypersphere under a general principle derived from maximum likelihood, HYPER-SET pursues distributional uniformity in the low-dimensional subspaces while promoting directional alignment with bases in the original high-dimensional space, constructing core Transformer components with intrinsic interpretability. Empirically, HYPER-SET matches or surpasses vanilla Transformers across diverse tasks with fewer parameters. Beyond a single architecture, our framework enables flexible design choices and scalable variants. This work contributes towards principled, more describable, and economical Transformer designs that are both theoretically motivated and practically effective. We discuss limitations and future directions in Appendix H.

References

Juan A Acebrón, Luis L Bonilla, Conrad J Pérez Vicente, Félix Ritort, and Renato Spigler. The kuramoto model: A simple paradigm for synchronization phenomena. *Reviews of modern physics*, 77(1):137–185, 2005. 5

David H Ackley, Geoffrey E Hinton, and Terrence J Sejnowski. A learning algorithm for boltzmann machines. *Cognitive science*, 9(1):147–169, 1985. 2

Brandon Amos and J Zico Kolter. Optnet: Differentiable optimization as a layer in neural networks. In *International conference on machine learning*, pp. 136–145. PMLR, 2017. 2

Brandon Amos, Ivan Jimenez, Jacob Sacks, Byron Boots, and J Zico Kolter. Differentiable mpc for end-to-end planning and control. *Advances in neural information processing systems*, 31, 2018. 2

Rohan Anil, Sebastian Borgeaud, Yonghui Wu, Jean-Baptiste Alayrac, Jiahui Yu, Radu Soricut, Johan Schalkwyk, Andrew M Dai, Anja Hauth, Katie Millican, et al. Gemini: A family of highly capable multimodal models. *arXiv preprint arXiv:2312.11805*, 1, 2023. 1

Thomas Bachlechner, Bodhisattwa Prasad Majumder, Henry Mao, Gary Cottrell, and Julian McAuley. Rezero is all you need: Fast convergence at large depth. In *Uncertainty in Artificial Intelligence*, pp. 1352–1361. PMLR, 2021. 6

Sangmin Bae, Adam Fisch, Hrayr Harutyunyan, Ziwei Ji, Seungyeon Kim, and Tal Schuster. Relaxed recursive transformers: Effective parameter sharing with layer-wise loRA. In *The Thirteenth International Conference on Learning Representations*, 2025. URL https://openreview.net/forum?id=WwpYSOkkCt. 3, 10, 30

Shaojie Bai, J Zico Kolter, and Vladlen Koltun. Deep equilibrium models. *Advances in neural information processing systems*, 32, 2019. 2

Andrea Banino, Jan Balaguer, and Charles Blundell. Pondernet: Learning to ponder. In *8th ICML Workshop on Automated Machine Learning (AutoML)*, 2021. URL https://openreview.net/forum?id=1EuxRTe0WN. 7

Arpit Bansal, Avi Schwarzschild, Eitan Borgnia, Zeyad Emam, Furong Huang, Micah Goldblum, and Tom Goldstein. End-to-end algorithm synthesis with recurrent networks: Extrapolation without overthinking. *Advances in Neural Information Processing Systems*, 35:20232–20242, 2022. 3, 7

Hangbo Bao, Li Dong, Songhao Piao, and Furu Wei. BEit: BERT pre-training of image transformers. In *International Conference on Learning Representations*, 2022. URL https://openreview.net/forum?id=p-BhZSz59o4. 1

Trenton Bricken, Adly Templeton, Joshua Batson, Brian Chen, Adam Jermyn, Tom Conerly, Nick Turner, Cem Anil, Carson Denison, Amanda Askell, Robert Lasenby, Yifan Wu, Shauna Kravec, Nicholas Schiefer, Tim Maxwell, Nicholas Joseph, Zac Hatfield-Dodds, Alex Tamkin, Karina Nguyen, Brayden McLean, Josiah E Burke, Tristan Hume, Shan Carter, Tom Henighan, and Christopher Olah. Towards monosemanticity: Decomposing language models with dictionary learning. *Transformer Circuits Thread*, 2023. https://transformer-circuits.pub/2023/monosemantic-features/index.html. 1

Anthony Brohan, Noah Brown, Justice Carbajal, Yevgen Chebotar, Joseph Dabis, Chelsea Finn, Keerthana Gopalakrishnan, Karol Hausman, Alex Herzog, Jasmine Hsu, et al. Rt-1: Robotics transformer for real-world control at scale. *arXiv preprint arXiv:2212.06817*, 2022. 1

Tom Brown, Benjamin Mann, Nick Ryder, Melanie Subbiah, Jared D Kaplan, Prafulla Dhariwal, Arvind Neelakantan, Pranav Shyam, Girish Sastry, Amanda Askell, et al. Language models are few-shot learners. *Advances in neural information processing systems*, 33:1877–1901, 2020. 1

Huiwen Chang, Han Zhang, Lu Jiang, Ce Liu, and William T Freeman. Maskgit: Masked generative image transformer. In *Proceedings of the IEEE/CVF Conference on Computer Vision and Pattern Recognition*, pp. 11315–11325, 2022. 9, 25

Lili Chen, Kevin Lu, Aravind Rajeswaran, Kimin Lee, Aditya Grover, Misha Laskin, Pieter Abbeel, Aravind Srinivas, and Igor Mordatch. Decision transformer: Reinforcement learning via sequence modeling. *Advances in neural information processing systems*, 34:15084–15097, 2021. 1

Tianlong Chen, Zhenyu Zhang, Yu Cheng, Ahmed Awadallah, and Zhangyang Wang. The principle of diversity: Training stronger vision transformers calls for reducing all levels of redundancy. In *Proceedings of the IEEE/CVF Conference on Computer Vision and Pattern Recognition*, pp. 12020–12030, 2022. 5

Róbert Csordás, Kazuki Irie, and Jürgen Schmidhuber. The devil is in the detail: Simple tricks improve systematic generalization of transformers. *arXiv preprint arXiv:2108.12284*, 2021. 3

Róbert Csordás, Kazuki Irie, Jürgen Schmidhuber, Christopher Potts, and Christopher D Manning. MoEUT: Mixture-of-experts universal transformers. In *The Thirty-eighth Annual Conference on Neural Information Processing Systems*, 2024. URL https://openreview.net/forum?id=ZxVrkm7Bjl. 33

Guy Dar, Mor Geva, Ankit Gupta, and Jonathan Berant. Analyzing transformers in embedding space. In Anna Rogers, Jordan Boyd-Graber, and Naoaki Okazaki (eds.), *Proceedings of the 61st Annual Meeting of the Association for Computational Linguistics (Volume 1: Long Papers)*, pp. 16124–16170, Toronto, Canada, July 2023. Association for Computational Linguistics. doi: 10.18653/v1/2023.acl-long.893. URL https://aclanthology.org/2023.acl-long.893/. 5

Tim R. Davidson, Luca Falorsi, Nicola De Cao, Thomas Kipf, and Jakub M. Tomczak. Hyperspherical variational auto-encoders. *34th Conference on Uncertainty in Artificial Intelligence (UAI-18)*, 2018. 20

Anna Dawid and Yann LeCun. Introduction to latent variable energy-based models: a path toward autonomous machine intelligence. *Journal of Statistical Mechanics: Theory and Experiment*, 2024(10):104011, 2024. 2

Jacob Devlin, Ming-Wei Chang, Kenton Lee, and Kristina Toutanova. BERT: Pre-training of deep bidirectional transformers for language understanding. In Jill Burstein, Christy Doran, and Thamar Solorio (eds.), *Proceedings of the 2019 Conference of the North American Chapter of the Association for Computational Linguistics: Human Language Technologies, Volume 1 (Long and Short Papers)*, pp. 4171–4186, Minneapolis, Minnesota, June 2019. Association for Computational Linguistics. doi: 10.18653/v1/N19-1423. URL https://aclanthology.org/N19-1423/. 1, 3

Yihe Dong, Jean-Baptiste Cordonnier, and Andreas Loukas. Attention is not all you need: pure attention loses rank doubly exponentially with depth. In Marina Meila and Tong Zhang (eds.), *Proceedings of the 38th International Conference on Machine Learning*, volume 139 of *Proceedings of Machine Learning Research*, pp. 2793–2803. PMLR, 18–24 Jul 2021. 5

Alexey Dosovitskiy, Lucas Beyer, Alexander Kolesnikov, Dirk Weissenborn, Xiaohua Zhai, Thomas Unterthiner, Mostafa Dehghani, Matthias Minderer, Georg Heigold, Sylvain Gelly, Jakob Uszkoreit, and Neil Houlsby. An image is worth 16x16 words: Transformers for image recognition at scale. In *International Conference on Learning Representations*, 2021. URL https://openreview.net/forum?id=YicbFdNTTy. 1

Yilun Du and Igor Mordatch. Implicit generation and modeling with energy based models. *Advances in Neural Information Processing Systems*, 32, 2019. 2

Yilun Du, Shuang Li, Joshua Tenenbaum, and Igor Mordatch. Learning iterative reasoning through energy minimization. In *International Conference on Machine Learning*, pp. 5570–5582. PMLR, 2022. 2, 7

Yilun Du, Jiayuan Mao, and Joshua B. Tenenbaum. Learning iterative reasoning through energy diffusion. In *International Conference on Machine Learning (ICML)*, 2024. 2

Abhimanyu Dubey, Abhinav Jauhri, Abhinav Pandey, Abhishek Kadian, Ahmad Al-Dahle, Aiesha Letman, Akhil Mathur, Alan Schelten, Amy Yang, Angela Fan, et al. The llama 3 herd of models. *arXiv preprint arXiv:2407.21783*, 2024. 1

Nelson Elhage, Neel Nanda, Catherine Olsson, Tom Henighan, Nicholas Joseph, Ben Mann, Amanda Askell, Yuntao Bai, Anna Chen, Tom Conerly, et al. A mathematical framework for transformer circuits. *Transformer Circuits Thread*, 1(1):12, 2021. 1

Jonas Geiping, Sean McLeish, Neel Jain, John Kirchenbauer, Siddharth Singh, Brian R Bartoldson, Bhavya Kailkhura, Abhinav Bhatele, and Tom Goldstein. Scaling up test-time compute with latent reasoning: A recurrent depth approach. *arXiv preprint arXiv:2502.05171*, 2025. 3, 33

Borjan Geshkovski, Cyril Letrouit, Yury Polyanskiy, and Philippe Rigollet. The emergence of clusters in self-attention dynamics. In *Thirty-seventh Conference on Neural Information Processing Systems*, 2023. URL https://openreview.net/forum?id=aMjaEkkXJx. 5

Mor Geva, Roei Schuster, Jonathan Berant, and Omer Levy. Transformer feed-forward layers are key-value memories. In Marie-Francine Moens, Xuanjing Huang, Lucia Specia, and Scott Wen-tau Yih (eds.), *Proceedings of the 2021 Conference on Empirical Methods in Natural Language Processing*, pp. 5484–5495, Online and Punta Cana, Dominican Republic, November 2021. Association for Computational Linguistics. doi: 10.18653/v1/2021.emnlp-main.446. URL https://aclanthology.org/2021.emnlp-main.446/. 5

Angeliki Giannou, Shashank Rajput, Jy-yong Sohn, Kangwook Lee, Jason D Lee, and Dimitris Papailiopoulos. Looped transformers as programmable computers. In *International Conference on Machine Learning*, pp. 11398–11442. PMLR, 2023. 3

Karol Gregor and Yann LeCun. Learning fast approximations of sparse coding. In *Proceedings of the 27th international conference on international conference on machine learning*, pp. 399–406, 2010. 3

Samuel Greydanus, Misko Dzamba, and Jason Yosinski. Hamiltonian neural networks. *Advances in neural information processing systems*, 32, 2019. 2

Andrey Gromov, Kushal Tirumala, Hassan Shapourian, Paolo Glorioso, and Daniel A Roberts. The unreasonable ineffectiveness of the deeper layers. *arXiv preprint arXiv:2403.17887*, 2024. 1

Xiaojun Guo, Yifei Wang, Tianqi Du, and Yisen Wang. Contranorm: A contrastive learning perspective on oversmoothing and beyond. In *The Eleventh International Conference on Learning Representations*, 2023. URL https://openreview.net/forum?id=SM7XkJouWHm. 26

Kaiming He, Xinlei Chen, Saining Xie, Yanghao Li, Piotr Dollár, and Ross Girshick. Masked autoencoders are scalable vision learners. In *Proceedings of the IEEE/CVF conference on computer vision and pattern recognition*, pp. 16000–16009, 2022. 1

Alex Henry, Prudhvi Raj Dachapally, Shubham Shantaram Pawar, and Yuxuan Chen. Query-key normalization for transformers. In Trevor Cohn, Yulan He, and Yang Liu (eds.), *Findings of the Association for Computational Linguistics: EMNLP 2020*, pp. 4246–4253, Online, November 2020. Association for Computational Linguistics. doi: 10.18653/v1/2020.findings-emnlp.379. URL https://aclanthology.org/2020.findings-emnlp.379/. 6

Martin Heusel, Hubert Ramsauer, Thomas Unterthiner, Bernhard Nessler, and Sepp Hochreiter. Gans trained by a two time-scale update rule converge to a local nash equilibrium. *Advances in neural information processing systems*, 30, 2017. 25

Benjamin Hoover, Yuchen Liang, Bao Pham, Rameswar Panda, Hendrik Strobelt, Duen Horng Chau, Mohammed Zaki, and Dmitry Krotov. Energy transformer. *Advances in Neural Information Processing Systems*, 36, 2024. 2, 7, 8, 26, 31, 32

John J Hopfield. Neural networks and physical systems with emergent collective computational abilities. *Proceedings of the national academy of sciences*, 79(8):2554–2558, 1982. 2

Edward J Hu, yelong shen, Phillip Wallis, Zeyuan Allen-Zhu, Yuanzhi Li, Shean Wang, Lu Wang, and Weizhu Chen. LoRA: Low-rank adaptation of large language models. In *International Conference on Learning Representations*, 2022. URL https://openreview.net/forum?id=nZeVKeeFYf9. 30

Jerry Yao-Chieh Hu, Thomas Lin, Zhao Song, and Han Liu. On computational limits of modern hopfield models: A fine-grained complexity analysis. In *International Conference on Machine Learning*, pp. 19327–19343. PMLR, 2024a. 3

Jerry Yao-Chieh Hu, Dennis Wu, and Han Liu. Provably optimal memory capacity for modern hopfield models: Transformer-compatible dense associative memories as spherical codes. In *The Thirty-eighth Annual Conference on Neural Information Processing Systems*, 2024b. URL https://openreview.net/forum?id=4UReW4Ez6s. 3

Yunzhe Hu, Difan Zou, and Dong Xu. An in-depth investigation of sparse rate reduction in transformer-like models. In *The Thirty-eighth Annual Conference on Neural Information Processing Systems*, 2024c. URL https://openreview.net/forum?id=CAC74VuMWX. 8, 26, 31

Robert Huben, Hoagy Cunningham, Logan Riggs Smith, Aidan Ewart, and Lee Sharkey. Sparse autoencoders find highly interpretable features in language models. In *The Twelfth International Conference on Learning Representations*, 2024. URL https://openreview.net/forum?id=F76bwRSLeK. 1

John Jumper, Richard Evans, Alexander Pritzel, Tim Green, Michael Figurnov, Olaf Ronneberger, Kathryn Tunyasuvunakool, Russ Bates, Augustin Žídek, Anna Potapenko, et al. Highly accurate protein structure prediction with alphafold. *nature*, 596(7873):583–589, 2021. 1

Pierre-Alexandre Kamienny, Stéphane d'Ascoli, Guillaume Lample, and François Charton. End-to-end symbolic regression with transformers. *Advances in Neural Information Processing Systems*, 35:10269–10281, 2022. 1

Jared Kaplan, Sam McCandlish, Tom Henighan, Tom B. Brown, Benjamin Chess, Rewon Child, Scott Gray, Alec Radford, Jeffrey Wu, and Dario Amodei. Scaling laws for neural language models, 2020. URL https://arxiv.org/abs/2001.08361. 1

George Em Karniadakis, Ioannis G Kevrekidis, Lu Lu, Paris Perdikaris, Sifan Wang, and Liu Yang. Physics-informed machine learning. *Nature Reviews Physics*, 3(6):422–440, 2021. 2

Md Kowsher, Nusrat Jahan Prottasha, Chun-Nam Yu, Ozlem Garibay, and Niloofar Yousefi. Does self-attention need separate weights in transformers? In Weizhu Chen, Yi Yang, Mohammad Kachuee, and Xue-Yong Fu (eds.), *Proceedings of the 2025 Conference of the Nations of the Americas Chapter of the Association for Computational Linguistics: Human Language Technologies (Volume 3: Industry Track)*, pp. 535–543, Albuquerque, New Mexico, April 2025. Association for Computational Linguistics. ISBN 979-8-89176-194-0. URL https://aclanthology.org/2025.naacl-industry.44/. 29

Leo Kozachkov, Ksenia V Kastanenka, and Dmitry Krotov. Building transformers from neurons and astrocytes. *Proceedings of the National Academy of Sciences*, 120(34):e2219150120, 2023. 3

Dmitry Krotov. A new frontier for hopfield networks. *Nature Reviews Physics*, 5(7):366–367, 2023. 22

Dmitry Krotov and John J Hopfield. Dense associative memory for pattern recognition. *Advances in neural information processing systems*, 29, 2016. 21

Dmitry Krotov and John J. Hopfield. Large associative memory problem in neurobiology and machine learning. In *International Conference on Learning Representations*, 2021. URL https://openreview.net/forum?id=X4y_10OX-hX. 2, 22

Vedang Lad, Wes Gurnee, and Max Tegmark. The remarkable robustness of llms: Stages of inference? *arXiv preprint arXiv:2406.19384*, 2024. 1

Zhenzhong Lan, Mingda Chen, Sebastian Goodman, Kevin Gimpel, Piyush Sharma, and Radu Soricut. Albert: A lite bert for self-supervised learning of language representations. In *International Conference on Learning Representations*, 2020. URL https://openreview.net/forum?id=H1eA7AEtvS. 1

Yann LeCun, Sumit Chopra, Raia Hadsell, et al. A tutorial on energy-based learning. 2006. 2

Tianhong Li, Huiwen Chang, Shlok Mishra, Han Zhang, Dina Katabi, and Dilip Krishnan. Mage: Masked generative encoder to unify representation learning and image synthesis. In *Proceedings of the IEEE/CVF Conference on Computer Vision and Pattern Recognition*, pp. 2142–2152, 2023. 9

Tianhong Li, Yonglong Tian, He Li, Mingyang Deng, and Kaiming He. Autoregressive image generation without vector quantization. In *The Thirty-eighth Annual Conference on Neural Information Processing Systems*, 2024. URL https://openreview.net/forum?id=VNBIF0gmkb. 9

Weiyang Liu, Rongmei Lin, Zhen Liu, Lixin Liu, Zhiding Yu, Bo Dai, and Le Song. Learning towards minimum hyperspherical energy. *Advances in neural information processing systems*, 31, 2018. 3, 5

Ziming Liu, Yixuan Wang, Sachin Vaidya, Fabian Ruehle, James Halverson, Marin Soljačić, Thomas Y Hou, and Max Tegmark. Kan: Kolmogorov-arnold networks. *arXiv preprint arXiv:2404.19756*, 2024. 3

Ilya Loshchilov and Frank Hutter. Decoupled weight decay regularization. In *International Conference on Learning Representations*, 2019. URL https://openreview.net/forum?id=Bkg6RiCqY7. 24

Ilya Loshchilov, Cheng-Ping Hsieh, Simeng Sun, and Boris Ginsburg. ngpt: Normalized transformer with representation learning on the hypersphere. *arXiv preprint arXiv:2410.01131*, 2024. 3

Xin Men, Mingyu Xu, Qingyu Zhang, Bingning Wang, Hongyu Lin, Yaojie Lu, Xianpei Han, and Weipeng Chen. Shortgpt: Layers in large language models are more redundant than you expect. *arXiv preprint arXiv:2403.03853*, 2024. 1

Kevin Meng, David Bau, Alex Andonian, and Yonatan Belinkov. Locating and editing factual associations in gpt. *Advances in Neural Information Processing Systems*, 35:17359–17372, 2022. 1

Takeru Miyato, Sindy Löwe, Andreas Geiger, and Max Welling. Artificial kuramoto oscillatory neurons. *arXiv preprint arXiv:2410.13821*, 2024. 5

Neel Nanda, Lawrence Chan, Tom Lieberum, Jess Smith, and Jacob Steinhardt. Progress measures for grokking via mechanistic interpretability. In *The Eleventh International Conference on Learning Representations*, 2023. URL https://openreview.net/forum?id=9XFSbDPmdW. 1

Catherine Olsson, Nelson Elhage, Neel Nanda, Nicholas Joseph, Nova DasSarma, Tom Henighan, Ben Mann, Amanda Askell, Yuntao Bai, Anna Chen, Tom Conerly, Dawn Drain, Deep Ganguli, Zac Hatfield-Dodds, Danny Hernandez, Scott Johnston, Andy Jones, Jackson Kernion, Liane Lovitt, Kamal Ndousse, Dario Amodei, Tom Brown, Jack Clark, Jared Kaplan, Sam McCandlish, and Chris Olah. In-context learning and induction heads. *Transformer Circuits Thread*, 2022. https://transformer-circuits.pub/2022/in-context-learning-and-induction-heads/index.html. 1

OpenAI, Josh Achiam, Steven Adler, Sandhini Agarwal, Lama Ahmad, Ilge Akkaya, Florencia Leoni Aleman, Diogo Almeida, Janko Altenschmidt, Sam Altman, Shyamal Anadkat, Red Avila, Igor Babuschkin, Suchir Balaji, Valerie Balcom, Paul Baltescu, Haiming Bao, Mohammad Bavarian, Jeff Belgum, Irwan Bello, Jake Berdine, Gabriel Bernadett-Shapiro, Christopher Berner, Lenny Bogdonoff, Oleg Boiko, Madelaine Boyd, Anna-Luisa Brakman, Greg Brockman, Tim Brooks, Miles Brundage, Kevin Button, Trevor Cai, Rosie Campbell, Andrew Cann, Brittany Carey, Chelsea Carlson, Rory Carmichael, Brooke Chan, Che Chang, Fotis Chantzis, Derek Chen, Sully Chen, Ruby Chen, Jason Chen, Mark Chen, Ben Chess, Chester Cho, Casey Chu, Hyung Won Chung, Dave Cummings, Jeremiah Currier, Yunxing Dai, Cory Decareaux, Thomas Degry, Noah Deutsch, Damien Deville, Arka Dhar, David Dohan, Steve Dowling, Sheila Dunning, Adrien Ecoffet, Atty Eleti, Tyna Eloundou, David Farhi, Liam Fedus, Niko Felix, Simón Posada Fishman, Juston Forte, Isabella Fulford, Leo Gao, Elie Georges, Christian Gibson, Vik Goel, Tarun Gogineni, Gabriel Goh, Rapha Gontijo-Lopes, Jonathan Gordon, Morgan

Grafstein, Scott Gray, Ryan Greene, Joshua Gross, Shixiang Shane Gu, Yufei Guo, Chris Hallacy, Jesse Han, Jeff Harris, Yuchen He, Mike Heaton, Johannes Heidecke, Chris Hesse, Alan Hickey, Wade Hickey, Peter Hoeschele, Brandon Houghton, Kenny Hsu, Shengli Hu, Xin Hu, Joost Huizinga, Shantanu Jain, Shawn Jain, Joanne Jang, Angela Jiang, Roger Jiang, Haozhun Jin, Denny Jin, Shino Jomoto, Billie Jonn, Heewoo Jun, Tomer Kaftan, Łukasz Kaiser, Ali Kamali, Ingmar Kanitscheider, Nitish Shirish Keskar, Tabarak Khan, Logan Kilpatrick, Jong Wook Kim, Christina Kim, Yongjik Kim, Jan Hendrik Kirchner, Jamie Kiros, Matt Knight, Daniel Kokotajlo, Łukasz Kondraciuk, Andrew Kondrich, Aris Konstantinidis, Kyle Kosic, Gretchen Krueger, Vishal Kuo, Michael Lampe, Ikai Lan, Teddy Lee, Jan Leike, Jade Leung, Daniel Levy, Chak Ming Li, Rachel Lim, Molly Lin, Stephanie Lin, Mateusz Litwin, Theresa Lopez, Ryan Lowe, Patricia Lue, Anna Makanju, Kim Malfacini, Sam Manning, Todor Markov, Yaniv Markovski, Bianca Martin, Katie Mayer, Andrew Mayne, Bob McGrew, Scott Mayer McKinney, Christine McLeavey, Paul McMillan, Jake McNeil, David Medina, Aalok Mehta, Jacob Menick, Luke Metz, Andrey Mishchenko, Pamela Mishkin, Vinnie Monaco, Evan Morikawa, Daniel Mossing, Tong Mu, Mira Murati, Oleg Murk, David Mély, Ashvin Nair, Reiichiro Nakano, Rajeev Nayak, Arvind Neelakantan, Richard Ngo, Hyeonwoo Noh, Long Ouyang, Cullen O'Keefe, Jakub Pachocki, Alex Paino, Joe Palermo, Ashley Pantuliano, Giambattista Parascandolo, Joel Parish, Emy Parparita, Alex Passos, Mikhail Pavlov, Andrew Peng, Adam Perelman, Filipe de Avila Belbute Peres, Michael Petrov, Henrique Ponde de Oliveira Pinto, Michael, Pokorny, Michelle Pokrass, Vitchyr H. Pong, Tolly Powell, Alethea Power, Boris Power, Elizabeth Proehl, Raul Puri, Alec Radford, Jack Rae, Aditya Ramesh, Cameron Raymond, Francis Real, Kendra Rimbach, Carl Ross, Bob Rotsted, Henri Roussez, Nick Ryder, Mario Saltarelli, Ted Sanders, Shibani Santurkar, Girish Sastry, Heather Schmidt, David Schnurr, John Schulman, Daniel Selsam, Kyla Sheppard, Toki Sherbakov, Jessica Shieh, Sarah Shoker, Pranav Shyam, Szymon Sidor, Eric Sigler, Maddie Simens, Jordan Sitkin, Katarina Slama, Ian Sohl, Benjamin Sokolowsky, Yang Song, Natalie Staudacher, Felipe Petroski Such, Natalie Summers, Ilya Sutskever, Jie Tang, Nikolas Tezak, Madeleine B. Thompson, Phil Tillet, Amin Tootoonchian, Elizabeth Tseng, Preston Tuggle, Nick Turley, Jerry Tworek, Juan Felipe Cerón Uribe, Andrea Vallone, Arun Vijayvergiya, Chelsea Voss, Carroll Wainwright, Justin Jay Wang, Alvin Wang, Ben Wang, Jonathan Ward, Jason Wei, CJ Weinmann, Akila Welihinda, Peter Welinder, Jiayi Weng, Lilian Weng, Matt Wiethoff, Dave Willner, Clemens Winter, Samuel Wolrich, Hannah Wong, Lauren Workman, Sherwin Wu, Jeff Wu, Michael Wu, Kai Xiao, Tao Xu, Sarah Yoo, Kevin Yu, Qiming Yuan, Wojciech Zaremba, Rowan Zellers, Chong Zhang, Marvin Zhang, Shengjia Zhao, Tianhao Zheng, Juntang Zhuang, William Zhuk, and Barret Zoph. Gpt-4 technical report, 2024. URL https://arxiv.org/abs/2303.08774. 1

Maxime Oquab, Timothée Darcet, Théo Moutakanni, Huy V. Vo, Marc Szafraniec, Vasil Khalidov, Pierre Fernandez, Daniel HAZIZA, Francisco Massa, Alaaeldin El-Nouby, Mido Assran, Nicolas Ballas, Wojciech Galuba, Russell Howes, Po-Yao Huang, Shang-Wen Li, Ishan Misra, Michael Rabbat, Vasu Sharma, Gabriel Synnaeve, Hu Xu, Herve Jegou, Julien Mairal, Patrick Labatut, Armand Joulin, and Piotr Bojanowski. DINOv2: Learning robust visual features without supervision. *Transactions on Machine Learning Research*, 2024. ISSN 2835-8856. URL https://openreview.net/forum?id=a68SUt6zFt. Featured Certification. 1

Rasmus Palm, Ulrich Paquet, and Ole Winther. Recurrent relational networks. *Advances in neural information processing systems*, 31, 2018. 7, 10, 28

Vardan Papyan, Yaniv Romano, and Michael Elad. Convolutional neural networks analyzed via convolutional sparse coding. *Journal of Machine Learning Research*, 18(83):1–52, 2017. 3

Vardan Papyan, Yaniv Romano, Jeremias Sulam, and Michael Elad. Theoretical foundations of deep learning via sparse representations: A multilayer sparse model and its connection to convolutional neural networks. *IEEE Signal Processing Magazine*, 35(4):72–89, 2018. 3

William Peebles and Saining Xie. Scalable diffusion models with transformers. In *Proceedings of the IEEE/CVF International Conference on Computer Vision*, pp. 4195–4205, 2023. 1, 6

Hubert Ramsauer, Bernhard Schäfl, Johannes Lehner, Philipp Seidl, Michael Widrich, Lukas Gruber, Markus Holzleitner, Thomas Adler, David Kreil, Michael K Kopp, Günter Klambauer, Johannes Brandstetter, and Sepp Hochreiter. Hopfield networks is all you need. In *International*

Conference on Learning Representations, 2021. URL https://openreview.net/forum?id=tL89RnzIiCd. 2, 22

Olivier Roy and Martin Vetterli. The effective rank: A measure of effective dimensionality. In *2007 15th European signal processing conference*, pp. 606–610. IEEE, 2007. 26

Michael E. Sander, Pierre Ablin, Mathieu Blondel, and Gabriel Peyré. Sinkformers: Transformers with doubly stochastic attention. In Gustau Camps-Valls, Francisco J. R. Ruiz, and Isabel Valera (eds.), *Proceedings of The 25th International Conference on Artificial Intelligence and Statistics*, volume 151 of *Proceedings of Machine Learning Research*, pp. 3515–3530. PMLR, 28–30 Mar 2022. URL https://proceedings.mlr.press/v151/sander22a.html. 6

Nikunj Saunshi, Nishanth Dikkala, Zhiyuan Li, Sanjiv Kumar, and Sashank J. Reddi. Reasoning with latent thoughts: On the power of looped transformers. In *The Thirteenth International Conference on Learning Representations*, 2025. URL https://openreview.net/forum?id=din0lGfZFd. 3

Avi Schwarzschild, Eitan Borgnia, Arjun Gupta, Furong Huang, Uzi Vishkin, Micah Goldblum, and Tom Goldstein. Can you learn an algorithm? generalizing from easy to hard problems with recurrent networks. *Advances in Neural Information Processing Systems*, 34:6695–6706, 2021. 3, 7

Nir Shlezinger, Jay Whang, Yonina C Eldar, and Alexandros G Dimakis. Model-based deep learning. *Proceedings of the IEEE*, 111(5):465–499, 2023. 2

Jascha Sohl-Dickstein, Eric Weiss, Niru Maheswaranathan, and Surya Ganguli. Deep unsupervised learning using nonequilibrium thermodynamics. In Francis Bach and David Blei (eds.), *Proceedings of the 32nd International Conference on Machine Learning*, volume 37 of *Proceedings of Machine Learning Research*, pp. 2256–2265, Lille, France, 07–09 Jul 2015. PMLR. URL https://proceedings.mlr.press/v37/sohl-dickstein15.html. 2

Yang Song and Stefano Ermon. Generative modeling by estimating gradients of the data distribution. *Advances in neural information processing systems*, 32, 2019. 2

Qi Sun, Marc Pickett, Aakash Kumar Nain, and Llion Jones. Transformer layers as painters. *arXiv preprint arXiv:2407.09298*, 2024. 1

Shawn Tan, Yikang Shen, Zhenfang Chen, Aaron Courville, and Chuang Gan. Sparse universal transformer. In Houda Bouamor, Juan Pino, and Kalika Bali (eds.), *Proceedings of the 2023 Conference on Empirical Methods in Natural Language Processing*, pp. 169–179, Singapore, December 2023. Association for Computational Linguistics. doi: 10.18653/v1/2023.emnlp-main.12. URL https://aclanthology.org/2023.emnlp-main.12/. 33

Naftali Tishby and Noga Zaslavsky. Deep learning and the information bottleneck principle. In *2015 ieee information theory workshop (itw)*, pp. 1–5. IEEE, 2015. 5

Naftali Tishby, Fernando C Pereira, and William Bialek. The information bottleneck method. *arXiv preprint physics/0004057*, 2000. 5

Hugo Touvron, Matthieu Cord, Alexandre Sablayrolles, Gabriel Synnaeve, and Hervé Jégou. Going deeper with image transformers. In *Proceedings of the IEEE/CVF international conference on computer vision*, pp. 32–42, 2021. 6

Ruben S van Bergen and Nikolaus Kriegeskorte. Going in circles is the way forward: the role of recurrence in visual inference. *Current Opinion in Neurobiology*, 65:176–193, 2020. 3

Ashish Vaswani, Noam Shazeer, Niki Parmar, Jakob Uszkoreit, Llion Jones, Aidan N Gomez, Ł ukasz Kaiser, and Illia Polosukhin. Attention is all you need. In I. Guyon, U. Von Luxburg, S. Bengio, H. Wallach, R. Fergus, S. Vishwanathan, and R. Garnett (eds.), *Advances in Neural Information Processing Systems*, volume 30. Curran Associates, Inc., 2017. URL https://proceedings.neurips.cc/paper_files/paper/2017/file/3f5ee243547dee91fbd053c1c4a845aa-Paper.pdf. 1

Jesse Vig, Sebastian Gehrmann, Yonatan Belinkov, Sharon Qian, Daniel Nevo, Yaron Singer, and Stuart Shieber. Investigating gender bias in language models using causal mediation analysis. *Advances in neural information processing systems*, 33:12388–12401, 2020. 1

Guan Wang, Jin Li, Yuhao Sun, Xing Chen, Changling Liu, Yue Wu, Meng Lu, Sen Song, and Yasin Abbasi Yadkori. Hierarchical reasoning model. *arXiv preprint arXiv:2506.21734*, 2025. 7

Kevin Ro Wang, Alexandre Variengien, Arthur Conmy, Buck Shlegeris, and Jacob Steinhardt. Interpretability in the wild: a circuit for indirect object identification in GPT-2 small. In *The Eleventh International Conference on Learning Representations*, 2023. URL https://openreview.net/forum?id=NpsVSN6o4ul. 1

Po-Wei Wang, Priya Donti, Bryan Wilder, and Zico Kolter. Satnet: Bridging deep learning and logical reasoning using a differentiable satisfiability solver. In *International Conference on Machine Learning*, pp. 6545–6554. PMLR, 2019. 2, 24

Tongzhou Wang and Phillip Isola. Understanding contrastive representation learning through alignment and uniformity on the hypersphere. In *International conference on machine learning*, pp. 9929–9939. PMLR, 2020. 4

Zhou Wang, Eero P Simoncelli, and Alan C Bovik. Multiscale structural similarity for image quality assessment. In *The Thrity-Seventh Asilomar Conference on Signals, Systems & Computers, 2003*, volume 2, pp. 1398–1402. Ieee, 2003. 25

Zhou Wang, Alan C Bovik, Hamid R Sheikh, and Eero P Simoncelli. Image quality assessment: from error visibility to structural similarity. *IEEE transactions on image processing*, 13(4):600–612, 2004. 25

Dennis Wu, Jerry Yao-Chieh Hu, Teng-Yun Hsiao, and Han Liu. Uniform memory retrieval with larger capacity for modern hopfield models. In Ruslan Salakhutdinov, Zico Kolter, Katherine Heller, Adrian Weller, Nuria Oliver, Jonathan Scarlett, and Felix Berkenkamp (eds.), *Proceedings of the 41st International Conference on Machine Learning*, volume 235 of *Proceedings of Machine Learning Research*, pp. 53471–53514. PMLR, 21–27 Jul 2024a. URL https://proceedings.mlr.press/v235/wu24i.html. 3

Xinyi Wu, Amir Ajorlou, Zihui Wu, and Ali Jadbabaie. Demystifying oversmoothing in attention-based graph neural networks. *Advances in Neural Information Processing Systems*, 36, 2024b. 5

Jiacheng Xu and Greg Durrett. Spherical latent spaces for stable variational autoencoders. In Ellen Riloff, David Chiang, Julia Hockenmaier, and Jun'ichi Tsujii (eds.), *Proceedings of the 2018 Conference on Empirical Methods in Natural Language Processing*, pp. 4503–4513, Brussels, Belgium, October-November 2018. Association for Computational Linguistics. doi: 10.18653/v1/D18-1480. URL https://aclanthology.org/D18-1480/. 20

Yongyi Yang, Tang Liu, Yangkun Wang, Jinjing Zhou, Quan Gan, Zhewei Wei, Zheng Zhang, Zengfeng Huang, and David Wipf. Graph neural networks inspired by classical iterative algorithms. In *International Conference on Machine Learning*, pp. 11773–11783. PMLR, 2021. 3

Zhun Yang, Adam Ishay, and Joohyung Lee. Learning to solve constraint satisfaction problems with recurrent transformer. In *The Eleventh International Conference on Learning Representations*, 2023. URL https://openreview.net/forum?id=udNhDCr2KQe. 7

Yaodong Yu, Sam Buchanan, Druv Pai, Tianzhe Chu, Ziyang Wu, Shengbang Tong, Benjamin Haeffele, and Yi Ma. White-box transformers via sparse rate reduction. *Advances in Neural Information Processing Systems*, 36:9422–9457, 2023. 3, 4, 5, 7, 8, 9, 26, 31, 32

Alan L Yuille and Anand Rangarajan. The concave-convex procedure. *Neural computation*, 15(4): 915–936, 2003. 22

Biao Zhang and Rico Sennrich. Root mean square layer normalization. *Advances in Neural Information Processing Systems*, 32, 2019. 2

Richard Zhang, Phillip Isola, Alexei A Efros, Eli Shechtman, and Oliver Wang. The unreasonable effectiveness of deep features as a perceptual metric. In *Proceedings of the IEEE conference on computer vision and pattern recognition*, pp. 586–595, 2018. 25

A Theoretical Justification of Motivation

We provide here a theoretical foundation for the objective in Eq. 1, showing how it arises naturally from a maximum likelihood estimation (MLE) framework under mild assumptions.

Let $\boldsymbol{x} \in \mathbb{R}^d$ be a random vector (considered as a token in the context of Transformer) in a high-dimensional representation space with a probability distribution $p(\boldsymbol{x})$. Let $\{\boldsymbol{z}^h\}_{h=1}^H$ be a set of random vectors in low-dimensional latent spaces $\mathbb{R}^p$ $(p < d)$ with distinct support, following a prior joint probability distribution $p(z^1, \ldots, \boldsymbol{z}^H)$. We formulate information processing in the forward pass of neural networks as maximum likelihood estimation:

$$\max_{\boldsymbol{x}} \quad \mathbb{E}_{(\boldsymbol{z}^1,\ldots,\boldsymbol{z}^H)\sim p(\boldsymbol{z}^1,\ldots,\boldsymbol{z}^H)}\left[\log p(\boldsymbol{x}, \boldsymbol{z}^1, \ldots, \boldsymbol{z}^H; \theta, \phi)\right], \tag{13}$$

where θ and ϕ are parameters of the high- and low-dimensional encodings, respectively.

To make this optimization more tractable, we make the following basic and practical assumptions:

Assumption 1. *The random vectors $\boldsymbol{z}^1, \ldots, \boldsymbol{z}^H$ are independent and follow the identical distribution $p(\boldsymbol{z})$ in distinct latent spaces, i.e., $p(\boldsymbol{z}^1, \ldots, \boldsymbol{z}^H) = \Pi_{h=1}^H p(\boldsymbol{z}^h)$ and $p(\boldsymbol{z}^1) = \cdots = p(\boldsymbol{z}^H) = p(\boldsymbol{z})$.*

Assumption 2. *The prior distribution $p(\boldsymbol{z})$ is a uniform distribution with support on a hypersphere $\mathbb{S}^{p-1}$.*

Assumption 3. *The random vectors $(\boldsymbol{z}^1, \ldots, \boldsymbol{z}^H) \sim p_\phi(\boldsymbol{z}^1, \ldots, \boldsymbol{z}^H|\boldsymbol{x})$ from the posterior distribution are conditionally independent, i.e., $p_\phi(\boldsymbol{z}^1, \ldots, \boldsymbol{z}^H|\boldsymbol{x}) = \Pi_{h=1}^H p_\phi(\boldsymbol{z}^h|\boldsymbol{x})$.*

Assumption 2 of hyperspherical uniform distribution can be perceived to function as regularization on the latent representations to preserve maximum entropy and avoid representational collapse, which has been adopted to enhance auto-encoding (Xu & Durrett, 2018; Davidson et al., 2018). Under the above basic and practical assumptions, the MLE objective can be reformulated as:

$$\begin{aligned}
&\max_{\boldsymbol{x}} \quad \mathbb{E}_{(\boldsymbol{z}^1,\ldots,\boldsymbol{z}^H)\sim p(\boldsymbol{z}^1,\ldots,\boldsymbol{z}^H)}\left[\log p(\boldsymbol{x}, \boldsymbol{z}^1, \ldots, \boldsymbol{z}^H; \theta, \phi)\right] \\
&\quad = \mathbb{E}_{(\boldsymbol{z}^1,\ldots,\boldsymbol{z}^H)\sim p(\boldsymbol{z})}\left[\log p_\phi(\boldsymbol{z}^1, \ldots, \boldsymbol{z}^H|\boldsymbol{x})\right] + \mathbb{E}_{(\boldsymbol{z}^1,\ldots,\boldsymbol{z}^H)\sim p(\boldsymbol{z})}\left[\log p_\theta(\boldsymbol{x})\right] \\
&\quad = \sum_{h=1}^H \mathbb{E}_{\boldsymbol{z}^h\sim p(\boldsymbol{z})}\left[\log p_\phi(\boldsymbol{z}^h|\boldsymbol{x})\right] + \log p_\theta(\boldsymbol{x}) \\
&\quad = \sum_{h=1}^H \mathbb{E}_{\boldsymbol{z}^h\sim p(\boldsymbol{z})}\left[\log \frac{p_\phi(\boldsymbol{z}^h|\boldsymbol{x})}{p(\boldsymbol{z}^h)}\right] + \sum_{h=1}^H \mathbb{E}_{\boldsymbol{z}^h\sim p(\boldsymbol{z})}\left[\log p(\boldsymbol{z}^h)\right] + \log p_\theta(\boldsymbol{x}) \\
&\quad = \sum_{h=1}^H \mathbb{E}_{\boldsymbol{z}^h\sim p(\boldsymbol{z})}\left[\log \frac{p_\phi(\boldsymbol{z}^h|\boldsymbol{x})}{p(\boldsymbol{z})}\right] + \sum_{h=1}^H \mathbb{E}_{\boldsymbol{z}\sim p(\boldsymbol{z})}\left[\log p(\boldsymbol{z})\right] + \log p_\theta(\boldsymbol{x}) \\
&\quad = -\sum_{h=1}^H \mathrm{D}_{\mathrm{KL}}(p(\boldsymbol{z})\|p_\phi(\boldsymbol{z}^h|\boldsymbol{x})) - H \times \mathcal{H}(p(\boldsymbol{z})) + \log p_\theta(\boldsymbol{x}),
\end{aligned} \tag{14}$$

where $\mathrm{D}_{\mathrm{KL}}(\cdot\|\cdot)$ denotes Kullback-Leibler (KL) divergence and $\mathcal{H}(\cdot)$ means differential entropy. As the second term on entropy in Eq. 14 does not depend on variable $\boldsymbol{x}$, this objective ultimately reduces to Eq. 1 which we restate here for completeness:

$$\min_{\boldsymbol{x}} \quad \sum_{h=1}^H \underbrace{\mathrm{D}_{\mathrm{KL}}(p(\boldsymbol{z})\|p_\phi(\boldsymbol{z}^h|\boldsymbol{x}))}_{\text{uniformity}} \underbrace{- \log(p_\theta(\boldsymbol{x}))}_{\text{alignment}}.$$

The first term encourages the posterior $p_\phi(\boldsymbol{z}^h|\boldsymbol{x})$ defined on the vector $\boldsymbol{z}^h \in \mathbb{R}^p$ in latent space, which can be implemented by a transformation parameterized by ϕ, to approximate a uniform distribution on a hypersphere. To see why the second term implies alignment, suppose the distribution $p_\theta(\boldsymbol{x})$ is parameterized as a mixture of M von Mises–Fisher (vMF) distributions [7] with equal mixing

[7] https://en.wikipedia.org/wiki/Von_Mises–Fisher_distribution

coefficients:

$$-\log(p_\theta(\boldsymbol{x})) = -\log\left(\frac{1}{M}\sum_{m=1}^{M} f(\boldsymbol{x};\boldsymbol{\mu}_m,\kappa_m)\right) = -\log\left(\frac{1}{M}\sum_{m=1}^{M} C_d(\kappa_m)\exp(\kappa_m\boldsymbol{\mu}_m^T\boldsymbol{x})\right), \tag{15}$$

where $\boldsymbol{\mu}_m \in \mathbb{S}^{d-1}$ denotes mean direction on $(d-1)$-dimensional unit sphere and $\kappa_m \geq 0$ is the concentration parameter while $C_d(\kappa_m)$ is the normalization constant; therefore, finding the vector $\boldsymbol{x}$ that minimizes this negative log-probability Eq. 15 equals finding maximal inner product $\boldsymbol{\mu}_m^T\boldsymbol{x}$, thus aiming for directional alignment. In practice, the mean direction $\boldsymbol{\mu}_m$ is learned by backpropagation and consequently contains certain statistical properties from the data.

In summary, the objective Eq. 1 suggests that for a representation vector $\boldsymbol{x} \in \mathbb{R}^d$, the forward dynamics can be characterized by two complementary properties:

- **Mode Seeking**: Achieving semantic alignment with directional vectors encapsulating specific information derived from data in the **high-dimensional space**.
- **Mass Covering**: Maximally preserving the entropy embedded via regularizing distributional uniformity in the **low-dimensional space**.

These principles underpin our design of token dynamics, and we propose to use energy functions to quantify these two properties as instantiations that can induce various Transformer-based models.

B Preliminaries

B.1 Hopfield Networks

Given a network with N neurons $\boldsymbol{x} = [x_1, \ldots, x_N]$ that take binary values, the temporal evolution dynamics of these neurons are determined by a scalar-value energy function:

$$E = -\frac{1}{2}\sum_{i,j}\omega_{ij}x_ix_j = -\frac{1}{2}\boldsymbol{x}^T\boldsymbol{W}\boldsymbol{x}, \quad x_i, x_j \in \{+1, -1\}$$

where ω_{ij} represents the strength of connectivity between node x_i and x_j, and the connectivity is assumed to be symmetric, *i.e.*, $\omega_{ij} = \omega_{ji}$. We can further rewrite $\boldsymbol{W} = \sum_{i=1}^{P}\boldsymbol{\xi}_i\boldsymbol{\xi}_i^T$ as a set of patterns to be stored. The update rule of each node to retrieve the most relevant pattern follows the Hebbian learning rule used in neuroscience:

$$\boldsymbol{x}_{t+1} = \text{sign}(\boldsymbol{W}\boldsymbol{x}_t) = \text{sign}\left(\sum_{i=1}^{P}\boldsymbol{\xi}_i\boldsymbol{\xi}_i^T\boldsymbol{x}_t\right).$$

This update rule tends to minimize the energy function with retrieved patterns as its attractor. It is an embodiment of the idea of “Neurons that fire together wire together.”: If two neurons connect ($\omega_{ij} > 0$), then they should have the same state ($+1$ for active and -1 for dead). The number of patterns the network can store and retrieve is $\mathcal{O}(N)$.

B.2 Modern Continuous Hopfield Networks

To overcome the limitation of linear storage capacity, modern Hopfield networks, also known as Dense Associative Memory (Krotov & Hopfield, 2016), introduce nonlinearity in the energy and the update of neurons' states and make them suitable for continuous variables:

$$E = -\frac{1}{2}\sum_{i=1}^{P} f\left(\boldsymbol{\xi}_i^T\boldsymbol{x}\right), \; \boldsymbol{x}_{t+1} = \tanh\left(\sum_{i=1}^{P}\boldsymbol{\xi}_i f'\left(\boldsymbol{\xi}_i^T\boldsymbol{x}_t\right)\right),$$

where $\tanh(\cdot)$ is to ensure the neurons' states are constrained to the interval $[-1, 1]$ so that the energy is bounded from below. Depending on the form of f, the network could have power or exponential storage capacity. If we set $f(x) = x^2$, this reduces to the traditional networks with linear capacity.

If we further make modifications to the non-linearity in the energy function with $\mathrm{logsumexp}(\cdot)$, which is inspired by contrastive normalization, we can define the Modern Continuous Hopfield (MCH) energy function with a quadratic regularization term on $\boldsymbol{x}$:

$$E_{\text{MCH}} = -\log\left(\sum_{i=1}^{P} \exp\left(\boldsymbol{\xi}_{\boldsymbol{i}}^{T}\boldsymbol{x}\right)\right) + \frac{1}{2}\boldsymbol{x}^{T}\boldsymbol{x}. \tag{16}$$

By leveraging the concave-convex procedure (Yuille & Rangarajan, 2003), the update could be written as

$$\boldsymbol{x}_{t+1} = \Xi\,\mathrm{softmax}(\Xi^{T}\boldsymbol{x}_{t}),$$

where $\Xi = [\xi_1, \ldots, \xi_P] \in \mathbb{R}^{N\times P}$. This formulation has proven to converge to stationary points of the energy function E_{MCH}, and is linked to the key-value memory similar to the attention mechanism (Ramsauer et al., 2021). Notice that this update rule is essentially the cross-attention given a query vector $\boldsymbol{x}$ and can only describe the independent evolution of that vector. It fails to faithfully cover the parallel interactions between contextual tokens in the self-attention adopted in the GPT or BERT style Transformers.

The construction of the modern continuous Hopfield energy and update rule can also be carried out from a biologically plausible view by extending the network with hidden neurons and establishing a group of coupled differential equations. We refer the readers to (Krotov & Hopfield, 2021; Krotov, 2023) for more details.

C Derivation

C.1 Derivation of the Gradient of E_{ATTN}

$$\begin{aligned}
\dot{\boldsymbol{x}}_k &= -\nabla_{\boldsymbol{x}_k} E_{\text{ATTN}} \\
&= -\sum_{h=1}^{H}\left(\frac{\sum_{j=1}^{N}\boldsymbol{W}_h\boldsymbol{W}_h^T\boldsymbol{x}_j \exp\left(\beta(\boldsymbol{W}_h^T\boldsymbol{x}_k)^T(\boldsymbol{W}_h^T\boldsymbol{x}_j)\right)}{\sum_{j=1}^{N}\exp\left(\beta(\boldsymbol{W}_h^T\boldsymbol{x}_k)^T(\boldsymbol{W}_h^T\boldsymbol{x}_j)\right)} + \sum_{i=1}^{N}\frac{\boldsymbol{W}_h\boldsymbol{W}_h^T\boldsymbol{x}_i \exp\left(\beta(\boldsymbol{W}_h^T\boldsymbol{x}_i)^T(\boldsymbol{W}_h^T\boldsymbol{x}_k)\right)}{\sum_{j=1}^{N}\exp\left(\beta(\boldsymbol{W}_h^T\boldsymbol{x}_i)^T(\boldsymbol{W}_h^T\boldsymbol{x}_j)\right)}\right) \\
&= -\sum_{h=1}^{H}\Bigg(\boldsymbol{W}_h\boldsymbol{W}_h^T[\boldsymbol{x}_1,\ldots,\boldsymbol{x}_N]\begin{bmatrix}\exp\left(\beta(\boldsymbol{W}_h^T\boldsymbol{x}_k)^T(\boldsymbol{W}_h^T\boldsymbol{x}_1)\right)\\ \vdots \\ \exp\left(\beta(\boldsymbol{W}_h^T\boldsymbol{x}_k)^T(\boldsymbol{W}_h^T\boldsymbol{x}_N)\right)\end{bmatrix} \Big/ \sum_{j=1}^{N}\exp\left(\beta(\boldsymbol{W}_h^T\boldsymbol{x}_k)^T(\boldsymbol{W}_h^T\boldsymbol{x}_j)\right) + \\
&\qquad \sum_{i=1}^{N}\boldsymbol{W}_h\boldsymbol{W}_h^T\boldsymbol{x}_i\begin{bmatrix}\exp\left(\beta(\boldsymbol{W}_h^T\boldsymbol{x}_1)^T(\boldsymbol{W}_h^T\boldsymbol{x}_i)\right) / \sum_{j=1}^{N}\exp\left(\beta(\boldsymbol{W}_h^T\boldsymbol{x}_i)^T(\boldsymbol{W}_h^T\boldsymbol{x}_j)\right)\\ \vdots \\ \exp\left(\beta(\boldsymbol{W}_h^T\boldsymbol{x}_N)^T(\boldsymbol{W}_h^T\boldsymbol{x}_i)\right) / \sum_{j=1}^{N}\exp\left(\beta(\boldsymbol{W}_h^T\boldsymbol{x}_i)^T(\boldsymbol{W}_h^T\boldsymbol{x}_j)\right)\end{bmatrix}_k\Bigg) \\
&= -\sum_{h=1}^{H}\left(\boldsymbol{W}_h\boldsymbol{W}_h^T\boldsymbol{X}\underbrace{\mathrm{softmax}}_{\text{column}}\left(\beta(\boldsymbol{W}_h^T\boldsymbol{X})^T(\boldsymbol{W}_h^T\boldsymbol{x}_k)\right) + \sum_{i=1}^{N}\boldsymbol{W}_h\boldsymbol{W}_h^T\boldsymbol{x}_i\underbrace{\mathrm{softmax}}_{\text{column}}\left(\beta(\boldsymbol{W}_h^T\boldsymbol{X})^T(\boldsymbol{W}_h^T\boldsymbol{x}_i)\right)_k\right) \\
&= -\sum_{h=1}^{H}\left(\boldsymbol{W}_h\boldsymbol{W}_h^T\boldsymbol{X}\underbrace{\mathrm{softmax}}_{\text{column}}\left(\beta(\boldsymbol{W}_h^T\boldsymbol{X})^T(\boldsymbol{W}_h^T\boldsymbol{x}_k)\right) + \boldsymbol{W}_h\boldsymbol{W}_h^T\boldsymbol{X}\underbrace{\mathrm{softmax}}_{\text{column}}\left(\beta(\boldsymbol{W}_h^T\boldsymbol{X})^T(\boldsymbol{W}_h^T\boldsymbol{X})\right)_{[k,:]}\right) \\
&= -\sum_{h=1}^{H}\left(\boldsymbol{W}_h\boldsymbol{W}_h^T\boldsymbol{X}\underbrace{\mathrm{softmax}}_{\text{column}}\left(\beta(\boldsymbol{W}_h^T\boldsymbol{X})^T(\boldsymbol{W}_h^T\boldsymbol{x}_k)\right) + \boldsymbol{W}_h\boldsymbol{W}_h^T\boldsymbol{X}\underbrace{\mathrm{softmax}}_{\text{row}}\left(\beta(\boldsymbol{W}_h^T\boldsymbol{X})^T(\boldsymbol{W}_h^T\boldsymbol{X})\right)_{[:,k]}\right) \\
&= -\sum_{h=1}^{H}\left(\boldsymbol{W}_h\boldsymbol{W}_h^T\boldsymbol{X}\underbrace{\mathrm{softmax}}_{\text{column}}\left(\beta(\boldsymbol{W}_h^T\boldsymbol{X})^T(\boldsymbol{W}_h^T\boldsymbol{x}_k)\right) + \boldsymbol{W}_h\boldsymbol{W}_h^T\boldsymbol{X}\underbrace{\mathrm{softmax}}_{\text{row}}\left(\beta(\boldsymbol{W}_h^T\boldsymbol{X})^T(\boldsymbol{W}_h^T\boldsymbol{X})\right)_{[:,k]}\right)
\end{aligned}$$

$$\begin{aligned}\dot{\boldsymbol{X}} &= [\dot{\boldsymbol{x}}_1, \dots, \dot{\boldsymbol{x}}_N] \\ &= -\nabla_{\boldsymbol{X}} E_{\text{ATTN}} \\ &= -\left((\boldsymbol{W}\boldsymbol{W}^T\boldsymbol{X} \underbrace{\text{softmax}}_{\text{column-wise}} (\beta(\boldsymbol{W}^T\boldsymbol{X})^T(\boldsymbol{W}^T\boldsymbol{X})) + \boldsymbol{W}\boldsymbol{W}^T\boldsymbol{X} \underbrace{\text{softmax}}_{\text{row-wise}} (\beta(\boldsymbol{W}^T\boldsymbol{X})^T(\boldsymbol{W}^T\boldsymbol{X})) \right)\end{aligned}$$

C.2 Derivation of the Gradient of E_{FF}

$$\begin{aligned}\dot{\boldsymbol{x}}_k &= -\nabla_{\boldsymbol{x}_k} E_{\text{FF}} \\ &= \sum_{m=1}^{M} \text{ReLU}(\boldsymbol{d}_m^T \boldsymbol{x}_k) \cdot \mathbb{I}(\boldsymbol{d}_m^T \boldsymbol{x}_k > 0) \cdot \boldsymbol{d}_m \\ &= \sum_{m=1}^{M} \text{ReLU}(\boldsymbol{d}_m^T \boldsymbol{x}_k) \boldsymbol{d}_m \\ &= [\boldsymbol{d}_1, \dots, \boldsymbol{d}_M] \begin{bmatrix} \text{ReLU}(\boldsymbol{d}_1^T \boldsymbol{x}_k) \\ \vdots \\ \text{ReLU}(\boldsymbol{d}_M^T \boldsymbol{x}_k) \end{bmatrix} \\ &= \boldsymbol{D}\,\text{ReLU}(\boldsymbol{D}^T \boldsymbol{x}_k)\end{aligned}$$

$$\dot{\boldsymbol{X}} = [\dot{\boldsymbol{x}}_1, \dots, \dot{\boldsymbol{x}}_N] = -\nabla_{\boldsymbol{X}} E_{\text{FF}} = \boldsymbol{D}\,\text{ReLU}(\boldsymbol{D}^T \boldsymbol{X})$$

D Detailed Experimental Setups and Model Configurations

D.1 Network to Learn Adaptive Step Sizes

We propose to learn adaptive step sizes $\boldsymbol{\alpha}_t, \boldsymbol{\gamma}_t \in \mathbb{R}^d$ given the current iteration $t \in [1, L]$, where L is the iteration number of the layer with unique parameters, and the initial token $\boldsymbol{x}(0) \in \mathbb{R}^d$, using the network shown in Figure 7 and configurations in Table 6.

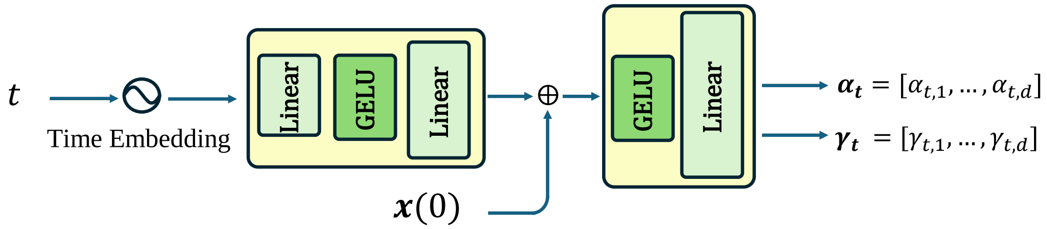
t
Time Embedding
Linear
GELU
Linear
⊕
$\boldsymbol{x}(0)$
GELU
Linear
$\boldsymbol{\alpha_t} = [\alpha_{t,1}, \dots, \alpha_{t,d}]$
$\boldsymbol{\gamma_t} = [\gamma_{t,1}, \dots, \gamma_{t,d}]$

Figure 7: Illustration of time embedding conditioned on the input to learn adaptive step size.

Table 6: Model configurations of network to learn adaptive step sizes.

Layer	Configurations
Time embedding	512
Linear	512 $\times d$
GELU	–
Linear	$d \times d$
GELU	–
Linear	$d \times 2d$

D.2 Solving Sudoku

Solving a Sudoku puzzle requires filling a 9 × 9 board, with some digits (1-9) known and unknown entries marked as 0. The unknown entries must be filled with digits perfectly such that the board satisfies a certain rule, which can be seen as a logical reasoning task (Wang et al., 2019). We tackle this puzzle by predicting the digits to fill in, conditioned on the given digits. It can be viewed as a simplified masked modeling on synthetic data. Cross-entropy loss is computed exclusively on unknown entries. We train all models with 200 epochs, 16 batch size, AdamW (Loshchilov & Hutter, 2019) with 0.1 weight decay, and learning rate from 1e-4 with cosine decay. The hidden dimension is set to 768.

Tables 7 and 8 show the training recipe and model configurations for solving Sudoku. We train the model with 24 iterations and can evaluate beyond these iterations.

Table 7: Training recipe for solving Sudoku.

Configurations	Value
Epochs	200
Batch size	16
# GPU	1 Nvidia 3090
# Training samples	9k
# Evaluating samples	1k
Optimizer	AdamW
β_1,β_2	0.9, 0.95
Weight decay	0.1
Learning rate (lr)	1e-4
Lr decay	Cosine
Gradient clipping	1.0

Table 8: Model configurations for solving Sudoku.

Configurations	Value
Vocabulary size	10
Layer	1
Iterations L	24
Hidden dimension d	768
Feedforward ratio M	$4d$
Number of heads H	12
Positional encoding	Learnable
Time embedding condition	$\boldsymbol{X}_0$
Time embedding frequency	512
Number of parameters	5.20 M

D.3 Image Classification

Tables 9 and 10 present the training recipe and model configurations for image classification on CIFAR-10/100, while Tables 11 and 12 show those on ImageNet-100/1K. All models are trained with a learnable class token `[CLS]`. In practice, we use absolute sinusoidal positional encoding and adopt conditioning on $\boldsymbol{X}_t$ for performance reasons. Table 13 lists the configurations of different sizes, and it applies to other tasks as well.

Table 9: Training recipe for image classification on CIFAR-10/100.

Configurations	Value
Epochs	200
Batch size	128
# GPU	1 Nvidia 3090
# Training samples	50k
# Evaluating samples	10k
Optimizer	Adam
β_1,β_2	0.9, 0.999
Weight decay	5e-5
Max learning rate (lr)	1e-3
Min learning rate (lr)	1e-5
Lr decay	Cosine
Warmup epochs	5
Input size	32

Table 10: Model configurations (`Small` Scaled-up) for image classification on CIFAR-10/100.

Configurations	Value
Patch size	8
Layer	1
Iterations L	12
Hidden dimension d	512
Feedforward ratio M	d
Number of heads H	8
Positional encoding	Sinusoidal
Time embedding condition	$\boldsymbol{X}_t$
Time embedding frequency	512

Table 11: Training recipe for image classification on ImageNet-100/1K.

Configurations	Value
Epochs	200
Batch size	256
# GPU	1 Nvidia A100
# Training samples	126,689/1,281,167
# Evaluating samples	5,000/50,000
Optimizer	Adam
β_1,β_2	0.9, 0.999
Weight decay	5e-5
Max learning rate (lr)	1e-3
Min learning rate (lr)	1e-5
Lr decay	Cosine
Warmup epochs	5
Input size	224

Table 12: Model configurations (`Small` Scaled-up) for image classification on ImageNet-100/1K.

Configurations	Value
Patch size	16
Layer	1
Iterations L	12
Hidden dimension d	512
Feedforward ratio M	d
Number of heads H	8
Positional encoding	Sinusoidal
Time embedding condition	$\boldsymbol{X}_t$
Time embedding frequency	512

Table 13: Model configurations of different sizes

Configurations	`Small`	`Small` Scale-up	`Base`
Hidden dimension d	384	512	768
Number of heads H	6	8	12

D.4 Masked Image Modeling

We follow (Chang et al., 2022) using VQ-VAE to tokenize the images to 16×16 latent code with the codebook size of 1024 after resizing the input to 256×256. The masking ratio is randomly chosen between $[0, 0.4]$, and the masked region is replaced by a learnable token. Training loss is computed only for the masked tokens. We also follow the iterative decoding process in (Chang et al., 2022) with temperature $= 1$ and decoding step $T = 24$. We also remove the MLP following the time embedding and set the embedding frequency equal to the hidden dimension to save parameters, and we find out that this implementation works better. Tables 14 and 15 show the detailed training recipe and configurations.

We evaluate the quality of the reconstructed images of masking out 40% of the images with `Base` configurations. We report Peak Signal-to-Noise Ratio (PSNR), Structural Similarity Index Measure (SSIM) (Wang et al., 2004), Multi-Scale SSIM (Wang et al., 2003), Learned Perceptual Image Patch Similarity (LPIPS) (Zhang et al., 2018) and Fréchet Inception Distance (FID) (Heusel et al., 2017) on the validation set (5k).

Table 14: Training recipe for masked image modeling.

Configurations	Value
Epochs	300
Batch size	256 (64 ×4)
# GPU	4 Nvidia 80 GB A100
# Training samples	126,689
# Evaluating samples	5,000
Optimizer	AdamW
β_1, β_2	0.9, 0.95
Weight decay	0.1
Learning rate (lr)	1e-4
Lr decay	None
Gradient clipping	3.0
Input size	256

Table 15: Model configurations for masked image modeling.

Configurations	Value
Vocabulary size	1025
Layer	1
Iterations	12
Hidden dimension d	768
Feedforward ratio M	d
Number of heads H	12
Positional encoding	Sinusoidal
Time embedding condition	$\boldsymbol{X}_0$
Time embedding frequency	768
Number of parameters	3.94 M

D.5 Definition of Effective Rank and Average Angle

We provide the formal definition of effective rank Eq. 17 and average angle Eq. 18 below. The effective rank is a continuous proxy of the full rank and, similar to the average angle, reflects the extent to which a set of vectors distributes uniformly.

Definition 1 (Effective Rank)**.** *For a matrix $\boldsymbol{X} \in \mathbb{R}^{d\times N}$, let $\Sigma = [\sigma_1, \dots, \sigma_r]$ be its singular values where r is its full rank and denote $p_i = \sigma_i / \sum_{j=1}^{r} \sigma_j$ the discrete probability. The effective rank (Roy & Vetterli, 2007; Guo et al., 2023) is defined as the exponential of the entropy*

$$\exp(-\sum_{i=1}^{r} p_i \log p_i). \tag{17}$$

Definition 2 (Average Angle)**.** *Given a set of vectors $\boldsymbol{X} = [\boldsymbol{x}_1, \dots, \boldsymbol{x}_N] \in \mathbb{R}^{d\times N}$, the average angle of these vectors is*

$$\arccos \frac{2}{N(N-1)} \sum_{i=1}^{N} \sum_{j=i+1}^{N} \frac{\boldsymbol{x}_i^T \boldsymbol{x}_j}{\|\boldsymbol{x}_i\|_2 \|\boldsymbol{x}_j\|_2}. \tag{18}$$

D.6 Comparisons of Parameter Efficiency and Computational Cost

To show the differences in parameters and computational cost incurred only by distinct architectures, we provide comparisons under the same width $d = 384$. Empirically, we compare FLOPs and runtime in one forward pass using `calflops`, measured on a single NVIDIA A100 GPU, of our model and other baselines with a $3 \times 224 \times 224$ random input.

Table 16: Comparisons of parameters and computational cost of different architectures.

Models	# Params	Memory	GFLOPs	Runtime (ms)
Transformer	2.38 M	528 MB	12.27	$4.99_{\pm 0.14}$
CRATE-T (Hu et al., 2024c)	0.91 M	528 MB	5.90	$4.61_{\pm 0.17}$
CRATE (Yu et al., 2023)	1.06 M	528 MB	5.90	$4.86_{\pm 0.19}$
Energy Transformer (Hoover et al., 2024)	1.50 M	670 MB	6.19	$21.95_{\pm 0.35}$
Ours	1.55 M	528 MB	6.81	$8.03_{\pm 0.21}$

Table 16 reports the results with mean and standard deviations averaged over 1,000 runs for robust measurements. Our model has fewer FLOPs as it has inherent structures like weight sharing due to mathematical design.

We further reveal via ablation shown in Table 17 that our bottleneck in runtime is largely because:

- we use an additional network to learn step sizes instead of keeping them fixed (∼ 2.33 ms),
- the current default implementation of `torch.nn.RMSNorm()`, which we use to meet the hyperspherical constraints, is slower than `torch.nn.LayerNorm()` (∼0.72 ms).

Currently, we trade some efficiency to allow for strong performance while keeping the principled design as transparent as possible with the additional modulation network for learned step sizes, which is adopted only for performance reasons rather than being a theoretically necessary component in our framework. In fact, our ablations that remove this extra network and fix the step sizes give similar runtime (5.70ms in Table 17), but the performance decreases greatly (81.45 on CIFAR-10 and 58.29 on CIFAR-100 in Table 4). So, we believe there is still room for improvement in optimizing the step sizes schedule and further enhancing this minimalist implementation in future work.

E Additional Results of Masked Image Modeling

Table 18 summarizes the results of masked image modeling with different masking ratios. When scaled to larger iterations and a wider feedforward module, our model achieves comparable results to Transformer but still slightly lags behind. This suggests the scalability of our model to large

Table 17: Bottleneck in runtime.

Models	# Params	GFLOPs	Runtime (ms)
Ours	1.55 M	6.81	$8.03_{\pm 0.21}$
Ours (Pre-Norm)	1.55 M	6.81	$8.05_{\pm 0.22}$
Ours (LayerNorm)	1.55 M	6.84	$7.31_{\pm 0.26}$
Ours (fixed step sizes)	0.91 M	4.98	$5.70_{\pm 0.15}$
Ours (Pre-Norm & LayerNorm)	1.55 M	6.82	$7.21_{\pm 0.28}$
Ours (fixed step sizes & Pre-Norm)	0.91 M	4.98	$5.53_{\pm 0.25}$
Ours (fixed step sizes & LayerNorm)	0.91 M	5.01	$4.86_{\pm 0.21}$
Ours (fixed step sizes & Pre-Norm & LayerNorm)	0.91 M	5.00	$4.74_{\pm 0.18}$

Table 18: Comparisons of masked image modeling performance of varied masking ratios.

Masking Ratios	Models	Layer / Iteration / FF Ratio M (# Params)	PSNR (↑)	SSIM (↑)	Multi-Scale SSIM (↑)	LPIPS (↓)	FID (↓)
10%	Transformer	L1 / Iter 12 / 4d (8.85 M)	**17.693**	**0.466**	**0.709**	0.236	**22.428**
	Ours	L1 / Iter 12 / d (3.94 M)	17.553	0.462	0.701	0.243	24.665
	Ours	L1 / Iter 24 / 8d (8.07 M)	17.673	0.465	0.708	**0.236**	22.517
20%	Transformer	L1 / Iter 12 / 4d (8.85 M)	**17.185**	**0.451**	**0.678**	**0.261**	**27.320**
	Ours	L1 / Iter 12 / d (3.94 M)	16.988	0.444	0.662	0.275	33.637
	Ours	L1 / Iter 24 / 8d (8.07 M)	17.170	0.450	0.676	0.262	28.120
30%	Transformer	L1 / Iter 12 / 4d (8.85 M)	**16.616**	**0.435**	**0.642**	**0.291**	**35.095**
	Ours	L1 / Iter 12 / d (3.94 M)	16.365	0.427	0.621	0.314	45.642
	Ours	L1 / Iter 24 / 8d (8.07 M)	16.590	0.434	0.638	0.294	35.128

configurations may be a bottleneck for its development and deployment. More visual comparisons are provided in Figure 8.

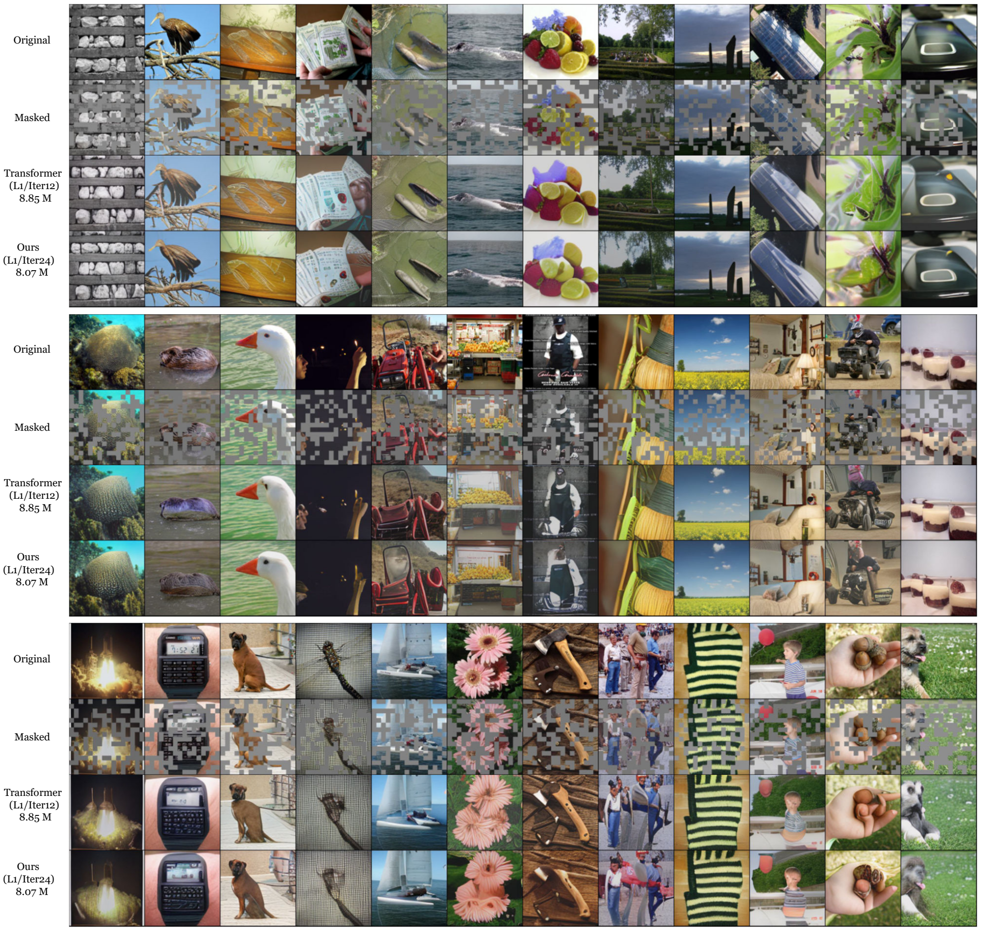

Figure 8: Visual comparisons of masked image modeling on ImageNet 256×256. Our model, when increased to Transformer scale with additional compute, can achieve similar reconstruction quality when masking ratio $= 40\%$.

F Rank and Average Angle of Each Head

F.1 Sudoku Dataset

Figures 9 and 10 capture the evolution of the effective rank and average angle of all heads. Most of them follow the separation dynamics on the hypersphere where tokens tend to be near-orthogonal, corroborating our design goal of attention energy.

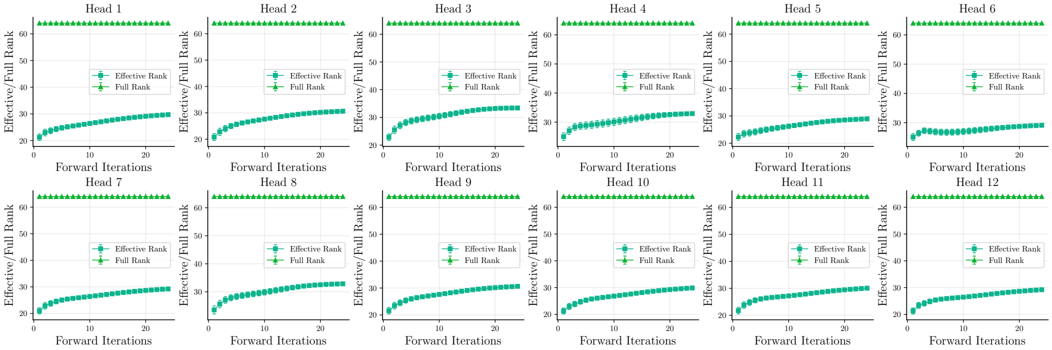

Figure 9: The effective rank of tokens projected to each subspace. Results are from the test set of Sudoku dataset (Palm et al., 2018).

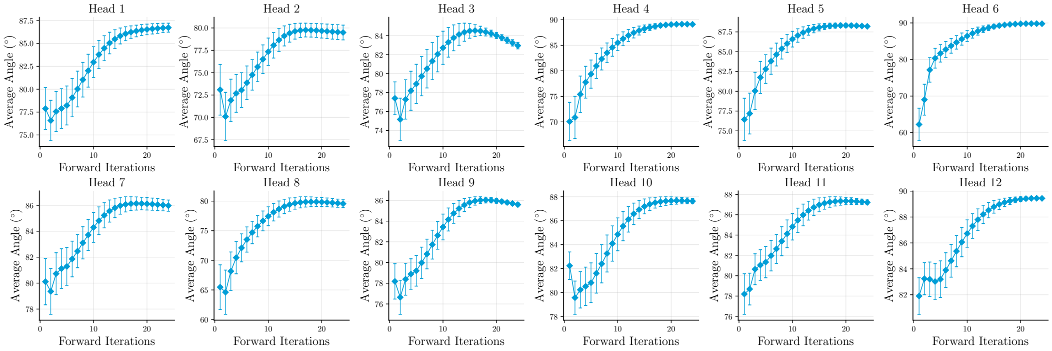

Figure 10: The average angle of tokens projected to each subspace. Results are from the test set of Sudoku dataset (Palm et al., 2018).

F.2 CIFAR-10 Dataset

The full results on CIFAR-10 also possess similar trends to those on the Sudoku dataset, as shown in Figures 11 and 12.

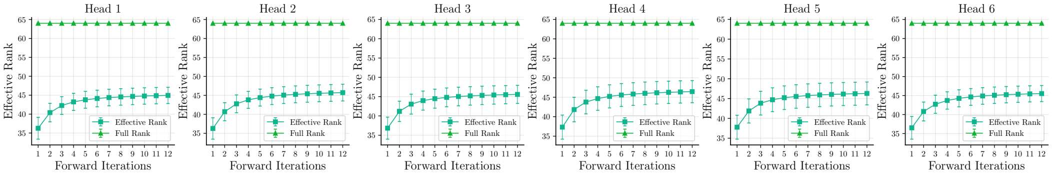

Figure 11: The effective rank of tokens projected to each subspace. Results are from CIFAR-10 validation set.

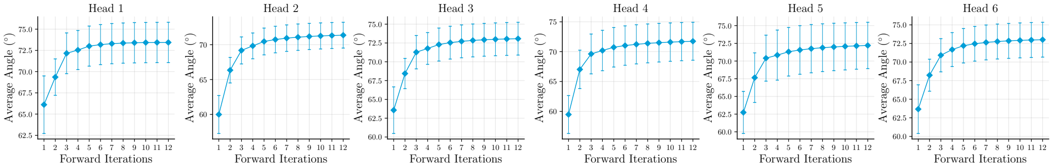

Figure 12: The average angle of tokens projected to each subspace. Results are from CIFAR-10 validation set.

F.3 Comparisons with Transformer with Shared Query, Key, and Value Matrix

A notable connection between Hyper-SET and vanilla Transformer lies in the shared query (Q), key (K), and value (V) projection matrix, which has been studied recently (Kowsher et al., 2025). To verify whether Hyper-SET captures essential Transformer behaviors, we adapt vanilla Transformer to have shared QKV projections and measure its effective rank and average angle among projected tokens. Furthermore, we also include comparisons with Hyper-SET that adopts fixed step sizes set as 0.1 to evaluate the necessity of learned ones.

As shown in Figures 13 and 14, both Hyper-SET and its fixed-step variant exhibit increasing token separation across subspaces, confirming the emergence of distributional uniformity and the benefit of learned step sizes. This dynamics is also mirrored in shared QKV Transformer, which cross-validates our insights on distributional uniformity in subspaces, suggesting the promise of this parameter-sharing design. In contrast, modifying the shared Transformer to reverse the update direction of attention—similar to the design in Eq. 9—leads to a decline in both rank and angle, highlighting a breakdown in uniformity. This contrast emphasizes that Hyper-SET is not a heuristic tweak of vanilla Transformer but a principled architecture.

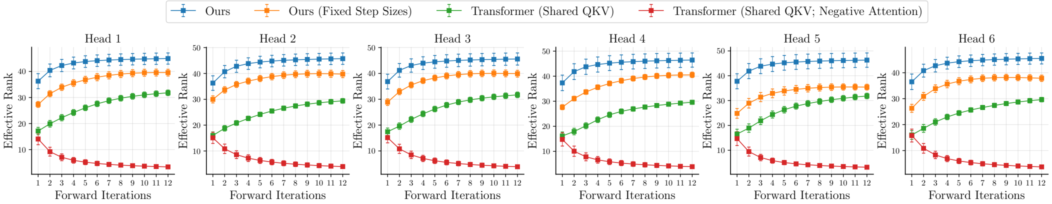

Figure 13: Comparisons of the effective rank at each subspace with fixed step sizes, Transformer with shared query/key/value matrix, and reverting the update sign before its attention. Results are from CIFAR-10 validation set.

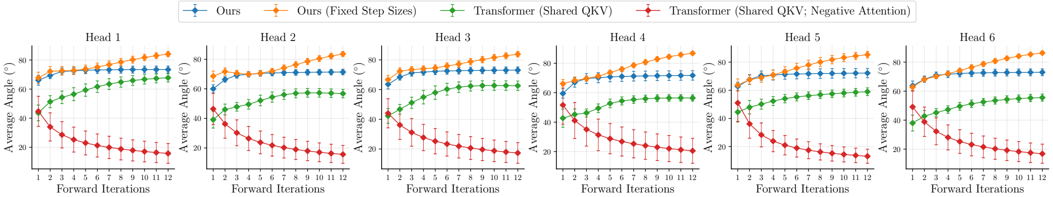

Figure 14: Comparisons of the average angle at each subspace with fixed step sizes, Transformer with shared query/key/value matrix, and reverting the update sign before its attention. Results are from CIFAR-10 validation set.

G Additional Results on Alternative Designs and Scalability

G.1 Alternative Designs on Energy Functions

Our proposed energy functions E_{ATTN} and E_{FF} provide an avenue to quantify the objective on uniformity and alignment in an amenable way for optimization. To manifest the significance of our conceptualization in designing a variety of Transformer-based models, we extend the energy functions to more general forms and provide alternative instantiations of them that can induce novel structures. Specifically, we generalize the energy functions in Eq. 3 and Eq. 5 to the following forms:

$$E_{\text{ATTN}} = \sum_{h=1}^{H} E_{\text{ATTN}}^{h} = \sum_{h=1}^{H}\sum_{i=1}^{N} f\left(\sum_{j=1}^{N} K(\boldsymbol{W}_h^T\boldsymbol{x}_i, \boldsymbol{W}_h^T\boldsymbol{x}_j)\right), \tag{19}$$

$$E_{\text{FF}} = -\sum_{i=1}^{N} g\left(\sum_{m=1}^{M} h(\boldsymbol{d}_m^T\boldsymbol{x}_i)\right). \tag{20}$$

where $K : \mathbb{R}^p \times \mathbb{R}^p \to \mathbb{R}$ is a kernel function and $f, g, h : \mathbb{R} \to \mathbb{R}$ are non-decreasing scalar functions. For clarity, we omit the hyperspherical constraint but its correspondence to $\mathrm{RMSNorm}$ still holds.

By choosing different variations on these functions, we arrive at alternative energy functions and their consequent attention and feedforward operators, of which we summarize the specifications in the following tables. Remarkably, in Table 19, we can derive an attention with linear complexity $\mathcal{O}(N)$ by specifying the kernel function with the inner product of an element-wise transformation $\Phi : \mathbb{R} \to \mathbb{R}$, bridging our energy view with recent advances in linear attention design. In practice, we choose it as the sigmoid function $\sigma(x) = 1/(1+\exp(-x))$, but other designs can also be possible. In Table 20, if we specify the outer function g in the feedforward energy as a quadratic function, there is a novel summation and a Hadamard product operation emerging with the transformation Φ, similar to the gating mechanism. We also specify Φ with the sigmoid function.

In summary, these design choices demonstrate that HYPER-SET is more than just a single model, but a blueprint for constructing principled Transformer variants. Each component—self-attention, feedforward, and normalization—can be systematically interpreted and designed within our energy minimization framework, providing a pathway for principled, modular innovation in sequence model architectures.

Table 19: Alternative designs on attention energy E_{ATTN} and the induced operators.

Operator	$f(x)$	$K(\boldsymbol{x},\boldsymbol{y})$	E_{ATTN}	$-\nabla_{\boldsymbol{X}} E_{\text{ATTN}}$
Bi-Softmax (Ours)	$\beta^{-1}\log(x)$	$\exp(\beta\boldsymbol{x}^T\boldsymbol{y})$	Eq. 3	Eq. 7
Sigmoid-Softmax	$\frac{\beta^{-1}}{2}x$	$\sigma(\beta\boldsymbol{x}^T\boldsymbol{y})$	$\frac{1}{2}\sum_{h=1}^{H}\sum_{i=1}^{N}\sum_{j=1}^{N}\sigma\left(\beta(\boldsymbol{W}_h^T\boldsymbol{x}_i)^T\boldsymbol{W}_h^T\boldsymbol{x}_j\right)\beta^{-1}$	$\sum_{h=1}^{H}\boldsymbol{W}_h\boldsymbol{W}_h^T\boldsymbol{X}\sigma(1-\sigma)\left(\beta(\boldsymbol{W}_h^T\boldsymbol{X})^T\boldsymbol{W}_h^T\boldsymbol{X}\right)$
Linear Attention	$\frac{\beta^{-1}}{2}x$	$\frac{1}{2}\left(\beta\Phi(\boldsymbol{x})^T\Phi(\boldsymbol{y})\right)^2$	$\frac{1}{4}\sum_{h=1}^{H}\sum_{i=1}^{N}\sum_{j=1}^{N}\left(\beta\Phi(\boldsymbol{W}_h^T\boldsymbol{x}_i)^T\Phi(\boldsymbol{W}_h^T\boldsymbol{x}_j)\right)^2\beta^{-1}$	$\sum_{h=1}^{H}\boldsymbol{W}_h\Phi'(\boldsymbol{W}_h^T\boldsymbol{X})\odot\left(\beta\Phi(\boldsymbol{W}_h^T\boldsymbol{X})\Phi(\boldsymbol{W}_h^T\boldsymbol{X})^T\Phi(\boldsymbol{W}_h^T\boldsymbol{X})\right)$

Table 20: Alternative designs on feedforward energy E_{FF} and the induced operators.

Operator	$g(x)$	$h(x)$	E_{FF}	$-\nabla_{\boldsymbol{X}} E_{\text{FF}}$
ReLU FF (Ours)	x	$\frac{1}{2}\,\mathrm{ReLU}^2(x)$	Eq. 5	Eq. 10
Softmax FF	$\log(x)$	$\exp(x)$	$-\sum_{i=1}^{N}\log\left(\sum_{m=1}^{M}\exp(\boldsymbol{d}_m^T\boldsymbol{x}_i)\right)$	$\boldsymbol{D}\underbrace{\mathrm{softmax}}_{\text{column-wise}}(\boldsymbol{D}^T\boldsymbol{X})$
Gated FF	$\frac{1}{2}x^2$	$\Phi(x)$	$-\frac{1}{2}\sum_{i=1}^{N}\left(\sum_{m=1}^{M}\Phi\left(\boldsymbol{d}_m^T\boldsymbol{x}_i\right)\right)^2$	$\boldsymbol{D}\underbrace{\Phi(\boldsymbol{D}^T\boldsymbol{X})}_{\text{column sum}}\odot\Phi'(\boldsymbol{D}^T\boldsymbol{X})$

G.2 PRELIMINARY RESULTS ON SCALABILITY

Setups for depth-wise flexible computation To equip our model with flexible computation while maintaining its core recurrence-based parameter sharing, we add an independent low-rank adaptation (Hu et al., 2022) matrix $W = AB$ to every iteration of the Transformer layer sharing the same base parameters. Inspired by but unlike depth-wise adaptation of pre-trained models in (Bae et al., 2025), we train the base parameters and the adaptation matrix together. Both matrix $A \in \mathbb{R}^{d\times r}, B \in \mathbb{R}^{r\times d}$ with rank r are initialized with Gaussain of 0.02 standard deviation. The scaling factor before the adaptation matrix is set as 4.

Scaling results on images To further demonstrate the capability of our model when scaling up its size, we perform a preliminary evaluation on image classification. Following the experimental setups in the main paper to configure the models with one layer and repeat with 12 iterations, we scale up the width of Transformer to 1152 and ours to 1536, resulting in similar parameter size.

Table 21: Top-1 accuracy for image classification when scaling up the model size. Our model surpasses other baselines while being parameter-efficient compared to vanilla Transformer.

Dataset	Models	Width d	# Params	Accuracy (%)
CIFAR-10	Transformer	1152	16.0 M	89.42
	CRATE (Yu et al., 2023)	1152	4.1 M	88.77
	Energy Transformer (Hoover et al., 2024)	1152	8.0 M	76.21
	Ours	1536	14.3 M	**90.62**
CIFAR-100	Transformer	1152	16.1 M	62.83
	CRATE (Yu et al., 2023)	1152	4.2 M	63.39
	Energy Transformer (Hoover et al., 2024)	1152	8.1 M	55.47
	Ours	1536	14.4 M	**66.30**

The result is presented in Table 21. These explorations showcase the potential of HYPER-SET in improving model capacity without significantly increasing the total parameter count.

Scaling results on texts We also provide the results for text classifications to show the potential of HYPER-SET. We use `bert-base-uncased` from Hugging Face as the tokenizer with a maximum sequence length of 128. The number of recurrence is set to 6 (L1R6) and width is set to 384. The training recipe is the same as the image classification in Table 9 except we train for 10 epochs. The results on `yelp_review_full` dataset, a 5-way classification task, are shown in Table 22.

Table 22: Top-1 accuracy for text classification on `yelp_review_full` dataset.

Models	Width d	# Params	Accuracy (%)
Transformer	384	13.49 M	60.09
CRATE-T (Hu et al., 2024c)	384	12.02 M	59.43
CRATE (Yu et al., 2023)	384	12.17 M	59.18
Energy Transformer (Hoover et al., 2024)	384	12.61 M	54.93
Ours	384	12.66 M	**60.75**

H DISCUSSION AND LIMITATIONS

H.1 CONNECTIONS AND DIFFERENCES WITH ENERGY TRANSFORMER

Both our HYPER-SET and ET (Hoover et al., 2024) are grounded in the idea of interpreting Transformer components as gradient flows that minimize an energy function. However, the two approaches diverge significantly in motivations, theoretical formulation, and architectural design.

- **Motivation**
  - **HYPER-SET**: centers on a dual objective of semantic alignment (mode seeking) and uniformity (mass covering) under hyperspherical constraints grounded in maximal likelihood estimation. The proposed Hopfield-style energy aims to quantify it into an optimizable objective and serves as a specific instantiation of this more general principle, which fundamentally differs from ET.
  - **ET**: maintains the mechanistic interpretation of associative memory and does not directly connect the energy formulation to any particular representational challenge. Moreover, ET adopts Hopfield energy more as a starting point than as a motivation-driven design.
- **Methodology**
  - **HYPER-SET**: provides a more rigorous formulation of energy minimization. Our energy functions are defined *directly* on tokens Eq. 6 under a hyperspherical constraint. This formulation enables us to derive $\mathrm{RMSNorm}$ as a natural outcome of energy minimization in low-dimensional subspaces Eq. 8.
  - **ET**: defines energy over pre-normalized tokens (see Eq.(1)(6) in (Hoover et al., 2024)) rather than tokens per se, bypassing the constrained optimization step. As a result, the role of normalization in ET is more heuristic than principled, following standard pre-norm practices rather than emerging from the underlying energy.

- **Implementations**
  - **HYPER-SET**: a) applies alternating minimization that results in attention and feedforward modules *sequentially*, reflecting the original Transformer structure; b) adopts adaptive, learnable step sizes conditioned on the input and iteration index Eq. 12, allowing the model to modulate its energy descent dynamically.
  - **ET**: a) performs energy updates via auto-differentiation that results in a *parallelized* fashion; b) uses fixed step sizes.
- **Emperical Verification**
  - **HYPER-SET**: a) confirms that the designed energy decreases in the forward pass in Figures 5 and 6; b) supports generalizations beyond softmax attention (*e.g.*, different energy functions leading to alternative attention schemes), as illustrated in Tables 19 and 20.
  - **ET**: a) does not offer such explicit verification, leaving it unclear whether its dynamics faithfully track the energy descent objectives; b) Additionally, HYPER-SET achieves competitive performance with vanilla Transformers on tasks such as image classification and inference (*e.g.*, Sudoku), whereas ET does not demonstrate comparable results in these domains.

H.2 Practical Implications and Broader Impact

- **Why Study This Model**: This work proposes a principled approach to Transformer design by modeling representation learning as an energy minimization on the hyperspace. Unlike prior efforts such as Energy Transformer (Hoover et al., 2024) and CRATE (Yu et al., 2023), which either diverge from their theoretical formulations or lack generality to derive new architectures, our model directly formulates energy functions on tokens with improved rigorousness, while supporting a spectrum of alternative designs.
- **Why CRATE Is a Fair Baseline**: CRATE (Yu et al., 2023) also pursues transparency and principled design, which shares a similar spirit with our goal, making it an appropriate baseline. While engineering-heavy ViTs may excel in benchmarks, they often involve significant redundancy. We aim to advance more compact, describable, and empirically competitive model design for next-generation architectures.
- **Interpretability**: We view the forward pass of HYPER-SET as a dynamical system. It features greater interpretability than vanilla Transformer in the sense that this dynamics is more readily describable and characterized by a meaningful quantity-the energy function-and grounded in well-established principles as maximum likelihood estimation. Beyond being merely conceptual, this dynamics is quantitatively verifiable, providing an interpretable and testable framework for understanding representation evolution.
- **A General Principle Beyond Canonical Hopfield Energy**: The Hopfield energy we employ in the main paper serves as one instantiation under the proposed general principle. Our formulation allows for broader energy-based designs—such as kernel-based alternatives to $\mathrm{logsumexp}$—enabling principled generalizations beyond standard attention mechanisms.

H.3 Limitations

While HYPER-SET offers a principled and empirically competitive formulation for Transformer design, it also comes with several limitations that highlight directions for future work:

- First, the choice of subspace in our conceptualization is less explored. The choice of uniform prior on the hypersphere in assumption 2 could be too strong in practice. Overly enforcing uniformity may be restrictive in some tasks. Moreover, the number of subspaces H and its dimension p are chosen heuristically. Their relationship, if any, with the real data distribution remains unclear.
- Second, the modulation network to learn step sizes introduces complexity. Although we use a modulation network to learn step sizes adaptively, tuning the configurations of this network still requires considerable effort. In addition, it introduces more computational complexity despite that the overall architecture is more parameter-efficient.
- Third, our experiments on scalability are still preliminary. We confirm competitive and superior performance on less than 20 million parameters and prove depth-wise LoRA scaling effec-

tiveness. However, extensions to truly large-scale settings—e.g., billion-level—have yet to be demonstrated.

H.4 Future Directions

We provide several promising future directions:

1. **Autoregressive Modeling**: Hyper-SET currently lacks a causal structure, limiting its use in autoregressive sequence modeling. Adapting to GPT-style models with causal masking is an important future step.
2. **Flow Matching and ODE Connections**: The iterative updates in Hyper-SET resemble neural ODEs, suggesting potential connections to flow matching techniques that may unify Transformer-based models with generative modeling.
3. **Scalability and Adaptive Computation**: Our initial results with depth-wise LoRA are promising but preliminary. Future work could explore dynamic iteration depth, inspired by latent space reasoning (Geiping et al., 2025), sparsity (Tan et al., 2023), and mixture-of-experts (Csordás et al., 2024).